Observational evidence of rapid chlorine activation by mountain waves above northern Scandinavia

S. Kühl,[1] A. Dörnbrack,[2] W. Wilms-Grabe,[1] B.-M. Sinnhuber,[3] U. Platt,[1] and T. Wagner[1]

Received 21 March 2004; revised 3 September 2004; accepted 4 October 2004; published 27 November 2004.

[1] The Global Ozone Monitoring Experiment (GOME) routinely maps atmospheric column densities of chlorine dioxide (OClO), an important indicator of chlorine activation. In previous studies it was shown that the level of OClO during polar winters is anticorrelated to synoptic-scale temperatures inside the polar vortex. Here we present observations of exceptionally fast chlorine activation by mesoscale polar stratospheric clouds during the mountain wave event above northern Scandinavia between 20 and 22 January 1997. The observed slant column densities of OClO in the area of the mountain wave activity increase from 0.6 * 10^{14} molec/cm^2 to 1.3 * 10^{14} molec/cm^2. Combining the GOME observations with radiative transfer calculations, the corresponding vertical column densities are derived, and by applying pressure and temperature profiles from mesoscale simulations, the mixing ratios for OClO and ClO at the different altitude levels are estimated. The vertical column densities of OClO indicate a level of chlorine activation that is about two times higher compared to the days before the mountain wave event, and the deduced mixing ratios for ClO imply that chlorine was almost completely activated over a wide altitude range. The area showing enhanced OClO values increased by approximately 750.000 km^2 which is more than 3% of the polar vortex area ($\approx$23.0 * 10^6 km^2). These observations are in good agreement with previous model studies, where comparable increases and areas of chlorine activation were calculated. The case of 21 January 1997 and similar GOME OClO observations in other Arctic winters confirm the importance of stratospheric mountain waves for the activation of chlorine species in the northern hemisphere. *INDEX TERMS:* 0340 Atmospheric Composition and Structure: Middle atmosphere—composition and chemistry; 0341 Atmospheric Composition and Structure: Middle atmosphere—constituent transport and chemistry (3334); 3329 Meteorology and Atmospheric Dynamics: Mesoscale meteorology; 3360 Meteorology and Atmospheric Dynamics: Remote sensing; *KEYWORDS:* GOME, mountain waves, chlorine activation

Citation: Kühl, S., A. Dörnbrack, W. Wilms-Grabe, B.-M. Sinnhuber, U. Platt, and T. Wagner (2004), Observational evidence of rapid chlorine activation by mountain waves above northern Scandinavia, *J. Geophys. Res.*, *109*, D22309, doi:10.1029/2004JD004797.

1. Introduction

[2] In the polar winter, stratospheric temperatures can fall below the threshold for formation of polar stratospheric clouds (PSCs). By heterogeneous reactions on PSC particles, the ozone-inert chlorine reservoirs (mainly $ClONO_2$ and HCl) are converted into ozone destroying species (active chlorine, mainly Cl, ClO and ClOOCl [see, e.g., *Solomon*, 1999]). This activation of chlorine initiates catalytic ozone destruction cycles like the ClO-ClOOCl and the ClO-BrO cycle [*Molina and Molina*, 1987; *McElroy et al.*, 1986].

[3] OClO (chlorine dioxide) is exclusively formed by reaction of ClO with BrO [*Toumi*, 1994]. The amount of OClO in an air mass therefore gives a good indication of the degree of chlorine activation, especially for solar zenith angles below 90 degrees [*Schiller and Wahner*, 1996; *Tornkvist et al.*, 2002]. Since OClO shows strong differential absorption features in the UV spectral range, it can be detected by means of Differential Optical Absorption Spectroscopy (DOAS) [*Solomon et al.*, 1987a; *Platt*, 1994].

[4] The growth of PSC-particles and their potential to activate chlorine species increases with lower temperatures [*Borrmann et al.*, 1997; *Peter*, 1997]. Long-lasting cold stratospheric temperatures occur regularly inside the stable polar vortex above the Antarctic. The Arctic polar vortex, however, is frequently disturbed by planetary wave activity. Therefore its intensity, size, shape, and lifetime vary significantly during the Arctic winter and from year to year [*Pawson et al.*, 1995; *Labitzke*, 1999].

[5] Mesoscale meteorological processes (=horizontal wavelengths below 2000 km) such as mountain waves [*Leutbecher and Volkert*, 1996; *Voigt et al.*, 2000; *Dörnbrack*

[1]Institut für Umweltphysik, Universität Heidelberg, Heidelberg, Germany.
[2]Institut für Physik der Atmosphäre, DLR Oberpfaffenhofen, Wessling, Germany.
[3]Institut für Umweltphysik, Universität Bremen, Bremen, Germany.

0148-0227/04/2004JD004797$09.00

et al., 2002] and jet stream generated inertia gravity waves [*Hitchman et al.*, 2003] cause stratospheric temperature anomalies by adiabatic cooling in the ascending branches of the waves. Since stratospheric temperatures in Arctic winters are often near the threshold for PSC-formation, adiabatic cooling due to stratospheric mountain waves can promote the formation of PSCs [*Deshler et al.*, 1994; *Voigt et al.*, 2000].

[6] It has been shown by model simulations from *Carslaw et al.* [1998] that mountain wave-induced PSCs can cause substantial chlorine activation. By theoretical calculations along mesoscale trajectories through mountain wave-induced PSCs with a chemical box model they determined that chlorine activation is significantly enhanced compared to the synoptic scale, leading to additional ozone depletion. Further studies by *Rivière et al.* [2000] and *Dörnbrack et al.* [2001] came to similar conclusions. Although measurements of mountain wave-induced PSCs have been reported [*Deshler et al.*, 1994; *Enell et al.*, 1999; *Wirth et al.*, 1999; *Dörnbrack et al.*, 1999; *Voigt et al.*, 2000, 2003], there are no observations of the corresponding chlorine activation.

[7] Satellite measurements of ClO [*Santee et al.*, 1995, 2003] and OClO [*Wagner et al.*, 2001] have displayed the dependency of stratospheric chlorine activation on meteorological conditions: The intensity, the beginning and duration, and the spatial extent of chlorine activation derived from GOME OClO measurements correlates well with the evolution of the stratospheric temperatures and the location of the polar vortex [*Wagner et al.*, 2001, 2002a; *Kühl et al.*, 2002; *Richter et al.*, 2004]. Therefore OClO column densities measured by GOME in the Arctic stratosphere show a strong annual variability [*Wagner et al.*, 2001; *Wilms-Grabe et al.*, 2002; *Kühl et al.*, 2004]. In contrast, OClO column densities above the Antarctic show the same magnitude and temporal evolution each year [*Wagner et al.*, 2001], with the exception of the winter 2002, where a major warming in September caused a rapid decrease of the observed OClO values [*Richter et al.*, 2004]. In both hemispheres, a strong anticorrelation exists between the GOME OClO column densities and the winter eddy heat flux [*Weber et al.*, 2003].

[8] These former studies of GOME OClO observations were devoted to large-scale features of chlorine activation that are associated with the overall chemical ozone loss during Arctic and Antarctic winters. The study at hand concentrates on GOME OClO measurements of significant stratospheric chlorine activation by mesoscale mountain waves above northern Scandinavia, which, to the best of our knowledge, are the first observational evidence for additional chlorine activation due to stratospheric mountain waves. By radiative transfer calculations the measured slant column densities (SCDs) are converted to vertical column densities (VCDs). Combining the satellite observations with mesoscale meteorological model simulations, we give an estimate for the increase in the level of chlorine activation at the respective altitude range by assuming different vertical profiles for the OClO mixing ratio.

[9] The paper is organized as follows. Section 2 describes the methods of observation and analyses used for this study. In section 3 we sketch the meteorological situation for the mountain wave event during 20–22 January 1997, and in section 4 we present the appendant GOME OClO observations. The increase in chlorine activation as a function of the altitude is investigated in section 5. Section 6 discusses the implications of the observations as well as the uncertainties of the measurement and the calculations, and the last section summarizes and concludes the paper.

2. Methods of Observations and Analyses

[10] The GOME instrument on board the ERS-2 satellite consists of a set of four spectrometers covering the wavelength range between 240 and 790 nm. It measures the intensities of the direct sunlight and of the light scattered back to the satellite from the Earth and its atmosphere in nadir view [see, e.g., *Burrows et al.*, 1999]. Because of the absorption by molecules in the light path through the atmosphere, the earthshine spectrum is attenuated, which can be described by the Beer-Lambert law:

$$I(\lambda) = I_0(\lambda) \exp\left(- \sum_i \sigma_i(\lambda) \int_0^L c_i(l) dl \right) = I_0(\lambda) \exp\left(- \sum_i \sigma_i(\lambda) S_i \right) \quad (1)$$

where σ_i is the absorption cross section of the i-th absorber with concentration c_i and $I(\lambda)$ and $I_0(\lambda)$ are the measured Sun and earthshine spectra (neglecting scattering processes, see below).

[11] By applying the DOAS method to these spectra, the integrated concentration c of an atmospheric absorber along the light path L, the slant column density (SCD) S, can be derived [*Platt*, 1994]. This algorithm simultaneously fits the SCDs S_j of several absorbers with known absorption cross sections $\sigma_j(\lambda)$ to the difference of the logarithm of the earthshine spectrum $I(\lambda)$ and a Fraunhofer reference $I_0(\lambda)$, which does not include the trace gas absorptions (e.g., the Sun spectrum).

[12] The absorptions due to tracegases show a strong variation with wavelength, which is described by the absorption cross sections of the considered molecules that are known from laboratory measurements. Rayleigh and Mie scattering, which (relative to the absorption of the tracegases) varies only slowly with wavelength, is accounted for by a broadband polynomial [*Platt*, 1994]. The difference between the logarithm of the earthshine spectra $I(\lambda)$ on one side and the logarithm of $I_0(\lambda)$ and the sum of the trace gas absorptions and the broadband polynomial on the other side is minimized by applying a least squares fit over all wavelengths λ [*Stutz and Platt*, 1996]:

$$\ln I(\lambda) - \left(\ln I_0(\lambda) - \sum_j S_j \sigma_j - \sum_p a_p \lambda^p \right) \rightarrow 0 \quad (2)$$

Developed mainly for monitoring of ozone, GOME is able to detect a range of atmospheric absorbers, among them NO_2, BrO, OClO, SO_2, HCHO, H_2O, O_2 and its dimer O_4 [*Burrows et al.*, 1999; *Wagner et al.*, 2002b]. For the OClO analysis, we use an earthshine spectrum at midlatitudes (containing no OClO absorption) as Fraunhofer reference

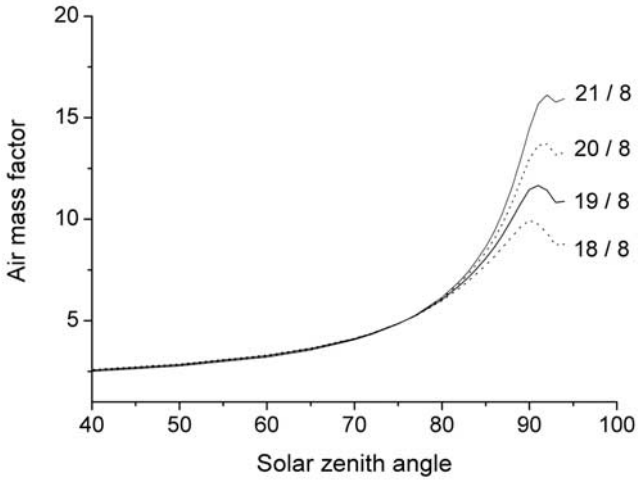

Figure 1. Air mass factors for OClO as a function of the solar zenith angle calculated by the radiative transfer model AMFTRAN for different gaussian vertical profiles of the OClO mixing ratio (Height of maximum and full width at half maximum in km as stated).

$I_0(\lambda)$, the OClO absorption cross section is taken from *Wahner et al.* [1987]. Details of the OClO-analysis of GOME spectra are described in *Wagner et al.* [2001]. Validation studies of GOME OClO measurements have been reported by *Wittrock et al.* [1999] and *Richter et al.* [1999]. These studies showed a good qualitative and quantitative agreement with ground based zenith-sky measurements of OClO.

[13] The ERS-2 satellite operates at an altitude of about 780 km in a Sun-synchronous, nearly polar orbit. While the satellite travels in an almost north-south direction on the daylight half of each orbit, the GOME instrument scans the surface in the perpendicular east-west direction. During one scan, three individual spectra are recorded, each corresponding to one of the three adjacent ground pixels. With a ground pixel size of 320 km (east-west) by 40 km (north-south) and up to 15 orbits per day, the whole global surface is covered in three days. For the polar regions (latitude $\phi > 70°$), a daily coverage is achieved. Thus the SCDs of OClO measured by GOME give a good overview of the intensity and the spatial extent of stratospheric chlorine activation [*Wagner et al.*, 2001, 2002a; *Wilms-Grabe et al.*, 2002; *Kühl et al.*, 2004].

[14] OClO observations are often presented as SCDs rather than as vertical column densities (VCDs) because of two main reasons. First, the conversion of SCDs to VCDs by

$$\mathrm{VCD} = \mathrm{SCD}/\mathrm{AMF}(\theta) \tag{3}$$

requires knowledge of the air mass factor (AMF), a quantity that describes the light path extension due to the slant viewing geometry [*Solomon et al.*, 1987b; *Marquard et al.*, 2000]. The AMF depends on the solar zenith angle (SZA) θ and the vertical profile of the considered absorbers and needs to be calculated with a radiative transfer model.

[15] Figure 1 shows AMFs for OClO calculated by the radiative transfer model AMFTRAN [*Marquard et al.*, 2000] for different vertical profiles of OClO. At large SZA ($\theta > 90°$), for which OClO measurements are typically analysed, the AMF depends strongly on the (often unknown) profile shape. For a detailed sensitivity study of the influence of several atmospheric factors on the GOME SCDs of OClO, see *Wagner et al.* [2001]. Second, also if converted to VCDs, the OClO observations can not be interpreted as a measurement of the chlorine activation level, since they still depend on the photolysis rate of OClO, which in turn strongly depends on the intensity of solar illumination and thereby also on the SZA.

[16] However, the substantial mountain wave induced enhancements in the GOME OClO SCDs discussed in this paper were measured at SZAs significantly lower than 90° ($\theta < 85°$). Therefore the AMF does not depend strongly on the vertical profile of OClO (see Figure 1) and the GOME SCD measurements can be converted into VCDs, although the actual OClO profile is not known. Likewise, the photolysis rate of OClO for low SZAs can be calculated with little uncertainty and the dependence of the OClO observations on its photochemistry can be accounted for in order to quantify the degree of chlorine activation from our observations (see section 5). Also, for these relatively low SZAs, the photolysis rate of OClO does not vary that strongly with the solar zenith angle as it does for e.g., $\theta > 90°$ (see Figure 2). Therefore it is not necessary to account for chemical enhancement and to apply a chemical air mass factor (for a solar zenith angle of 83°, the difference between the standard and the chemical AMF is less than 2%).

[17] For this study, photolysis frequencies of OClO were calculated by the photolysis model as used in the SLIMCAT chemical transport model [*Chipperfield*, 1999], which is based on *Lary and Pyle* [1991]. The model takes into account spherical geometry and multiple scattering. A coding error present in earlier versions of the original model [*Becker et al.*, 2000a, 2000b] has been corrected (M. Chipperfield, personal communication). OClO absorption cross sections are taken from *Wahner et al.* [1987]. Our standard calculations assumed an albedo of 0.3. Sensitivity calculations with albedos of 0.9 and 0.1 led to a variation of

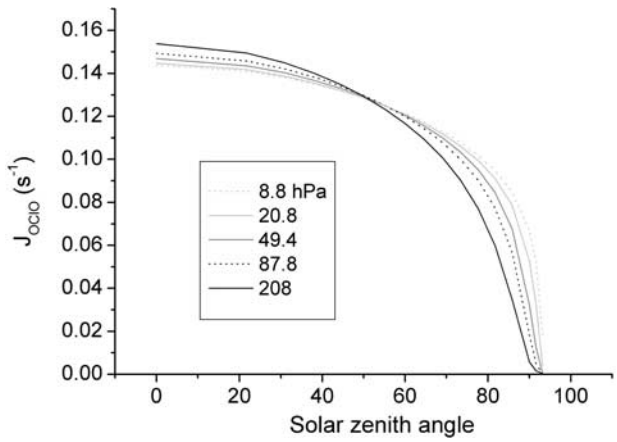

Figure 2. Photolysis frequency of OClO (J(OClO)) for different pressure levels calculated by a photolysis model based on *Lary and Pyle* [1991]. J(OClO) is plotted as a function of the solar zenith angle for five pressure levels between 210 and 8 hPa.

the OClO photolysis frequency of only about ±5% at a solar zenith angle of 83 degrees. As the maximum of the OClO absorption cross section is around 350 nm, there is little impact of the overhead ozone column on the OClO photolysis frequency. However, *Becker et al.* [2000a, 2000b] showed that an improved numerical solution of the radiative transfer equation leads to an increase of the OClO photolysis frequency by about 10% at a solar zenith angle of 60°. Figure 2 shows photolysis frequencies of OClO (J(OClO)) as a function of the solar zenith angle (SZA) for 5 pressure levels between 210 and 8 hPa. Especially for SZAs above 90°, J(OClO) drops rapidly, reaching values close to zero around SZA = 95°.

[18] Results of operational ECMWF synoptic-scale analyses and a mesoscale model simulation illustrate the meteorological setting and are utilized to estimate vertical profiles for the mountain wave induced chlorine activation. The mesoscale fields are calculated with the nonhydrostatic weather prediction model MM5-version 3.4 [*Dudhia*, 1993; *Dudhia et al.*, 2001]. The outer model domain is centred at (65°N, 20°E) with an extension of 2457 km × 2457 km. In this domain a horizontal grid size of $\Delta x = 27$ km is used. A local grid refinement scheme (nested domain with $\Delta x = 9$ km) is applied to resolve vertically propagating gravity waves with horizontal wavelengths less than 100 km. As shown by *Leutbecher and Volkert* [2000], the maximum horizontal wavelength resolved by the numerical code amounts to about $\approx 10\Delta x$, smaller wavelength are effectively damped by the numerical diffusion.

[19] The mesoscale simulation presented in this paper was performed with 148 vertical levels up to the model top at 10 hPa (≈30 km) which results in a high spatial resolution of $\Delta z \approx 200$ m. More important for the proper vertical propagation of mountain waves into the stratosphere is the modified radiative top boundary condition of *Zängl* [2002] which is applied in the current MM5 version. This boundary condition reduces the reflection at the model top significantly [*Dörnbrack et al.*, 2002]. Radiative and moist processes are switched off since the prime concern lies in the dynamics of mountain waves at upper levels. The initial conditions and boundary values of the model integration were prescribed by 6 hourly operational analyses of the ECMWF model with a horizontal resolution of 1.125° in latitude and longitude and 15 pressure levels between the surface and the 10 hPa pressure level.

[20] The mesoscale simulations, the radiative transfer calculations, and the GOME OClO measurements are combined to quantitatively investigate the effect of the mountain wave event on 21 January 1997 on the activation of stratospheric chlorine.

3. Meteorological Conditions During 20–22 January 1997

[21] During the late winter and spring 1996/1997 the polar vortex was very strong, cold and symmetric [*Coy et al.*, 1997]. GOME measurements of OClO reveal that chlorine activation started in early January and lasted until end of March [*Wagner et al.*, 2001], in consistency with observations from MLS and HALOE [*Santee et al.*, 1997; *Müller et al.*, 1997]. This persistence of high active chlorine levels until the end of the polar night resulted in substantial ozone loss [*Newman et al.*, 1997; *Manney et al.*, 1997; *Lefèvre et al.*, 1998; *Terao et al.*, 2002; *Tilmes et al.*, 2003].

[22] Figures 3a and 3b show the temperature at the 475 K isentropic surface (corresponding to ≈20 km altitude) based on T106 ECMWF operational analyses for 20 and 21 January 1997 at 1200 UT. Although the vortex was shifted off the pole it was only slightly elongated. On 21 January, temperatures were as low as 192 K, i.e., about 3 K below T_{NAT}, the threshold for formation of PSC type I, and about 4 K above the threshold T_{frost} for water ice (PSC type II) formation. For the whole month of January 1997, T106 ECMWF synoptic-scale temperatures never fell below T_{frost} at any altitude level.

[23] On the other hand, strong mountain wave activity above northern Scandinavia was reported for January 1997, especially during the period of 20–22 January [*Dörnbrack et al.*, 1999]. Above northern Scandinavia, minimum mesoscale temperatures fell below the frost point at all levels between 100 and 30 hPa on 21 January [*Dörnbrack et al.*, 2001]. Figure 3c shows simulated temperatures at the 475 K level based on the MM5 mesoscale model calculation. Also in the synoptic scale ECMWF analysis (Figure 3b), the effect of the mountain waves on the stratospheric temperatures can clearly be seen in the lee of the Scandinavian mountain ridge. However, in contrast to the rather homogeneous ECMWF temperature field, the mesoscale field consists of two nearly parallel stratospheric temperature anomalies aligned with the main Scandinavian mountain ridge. Their distance is about 600 km, resulting from the horizontal wavelength of the mountain waves.

[24] Inside the coldest areas, the simulated mesoscale temperature drops by $\Delta T = 11$ K below the ECMWF temperature ($T_{min} = 181$ K) and falls significantly below the threshold for formation of solid ice PSCs of $T_{frost} = 188$ K. These mesoscale simulation results are in accord with ground-based lidar observations of ice PSCs at Esrange, Sweden [*Fricke et al.*, 1997] and at Sodankylä, Finland [*Stein et al.*, 1999] as well as with other reported observations [*Dörnbrack et al.*, 1999] on this particular day.

4. GOME OClO Measurements

[25] Figure 4 shows the GOME measurements of OClO during the mountain wave period. On 20 January, high OClO SCDs (>1.3 * 10^{14} molec/cm^2) were observed which coincide with the shape of the polar vortex extending from north-western Greenland via northern Scandinavia to Russia (see Figure 3a). For the SZA of 90° (which at that time corresponds to a latitude of 70°N), maximum OClO SCDs of approximately 1.2 * 10^{14} molec/cm^2 are found, indicating that the vortex air masses were, considering the total column, moderately activated (in the cold Arctic winters 1995/96 and 1999/2000, GOME measured OClO SCDs larger than 2.0 * 10^{14} molec/cm^2 at the same SZA on 20 January [see *Wagner et al.*, 2001]). A comparison with the synoptic scale ECMWF temperatures reveals that temperatures inside the vortex had fallen below the threshold for PSC formation only since the beginning of January [*Coy et al.*, 1997; *Pawson and Naujokat*, 1999], which is rather late compared to other Arctic winters observed by GOME.

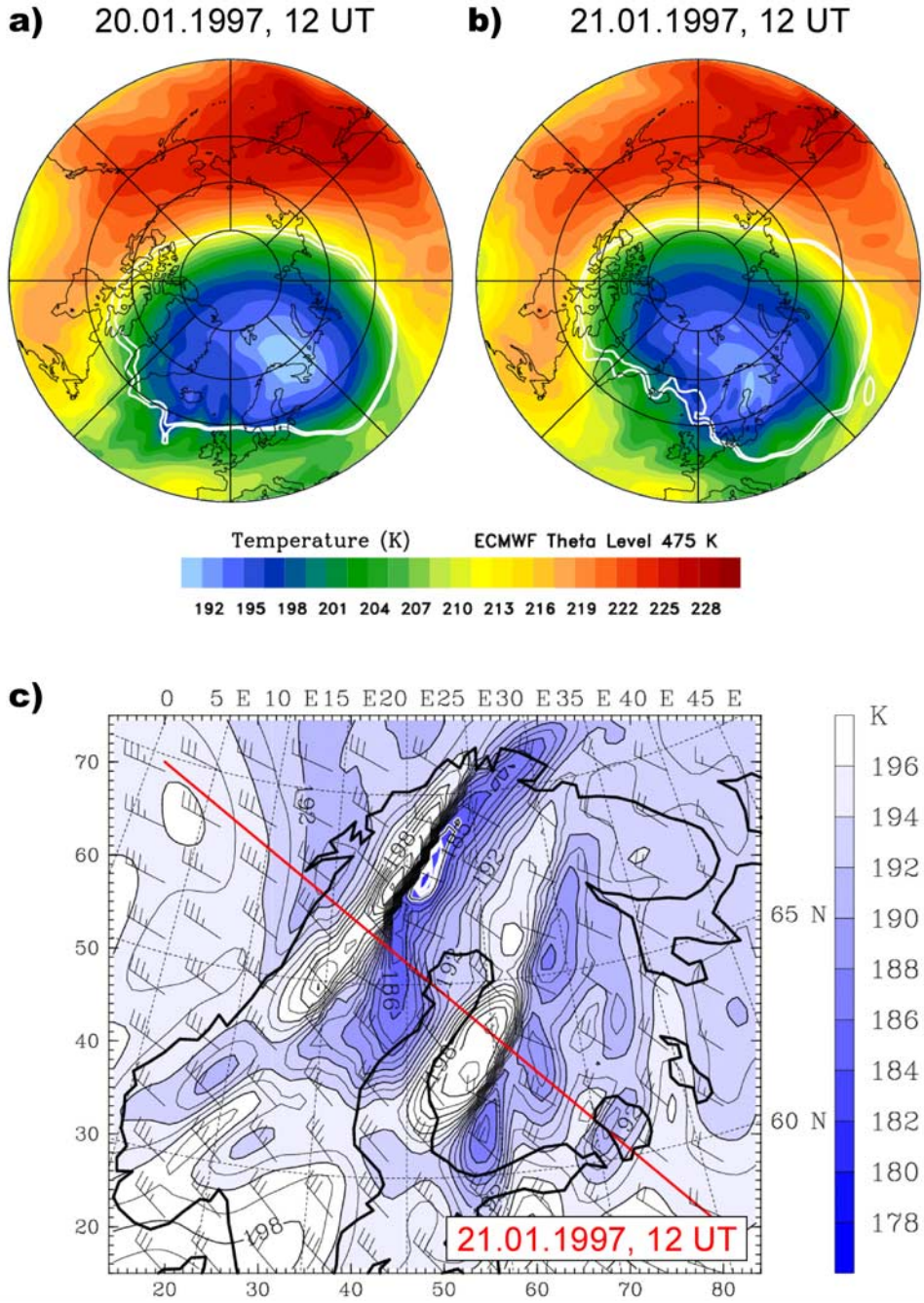

Figure 3. (a) Synoptic-scale temperatures of the 475 K isentropic surface (approximately 20 km height) based on the operational T106 ECMWF analysis for 20 January 1997, 1200 UT in K, color shaded. The white lines represent the edge of the polar vortex with values of 34 and 36 Potential Vorticity Units (PVU = 1×10^{-6} K kg^{-1} m^2 s^{-1}). (b) Same as Figure 3a for 21 January 1997. (c) Mesoscale temperatures at the 475 K isentropic surface on 21 January 1997, 1200 UT according to the MM5 analysis (T < 196 K, color shaded; K). Additional fields: Temperature isolines with $\Delta T = 1$ K (black lines), horizontal wind vectors (barbs; long: 10 ms^{-1}, short: 5 ms^{-1}). Numerical results are from the outer domain of the mesoscale model ($\Delta x = 27$ km). The red line indicates a path parallel to the wind direction, for which the mesoscale temperature profile is shown in Figure 7.

[26] For each GOME orbit, a decrease of the OClO SCDs toward lower latitudes (equivalent to lower SZAs) is seen, which results from a combination of various factors: First, the polar vortex and hence chlorine activated air masses are usually located at high latitudes. Second, it reflects the dependence of the OClO SCDs on the air mass factor and the photolysis frequency of OClO, which both lead to higher OClO SCDs for high SZAs (see section 2). For a quantitative comparison of OClO measurements at different SZAs, these effects have to be taken into account (see section 5).

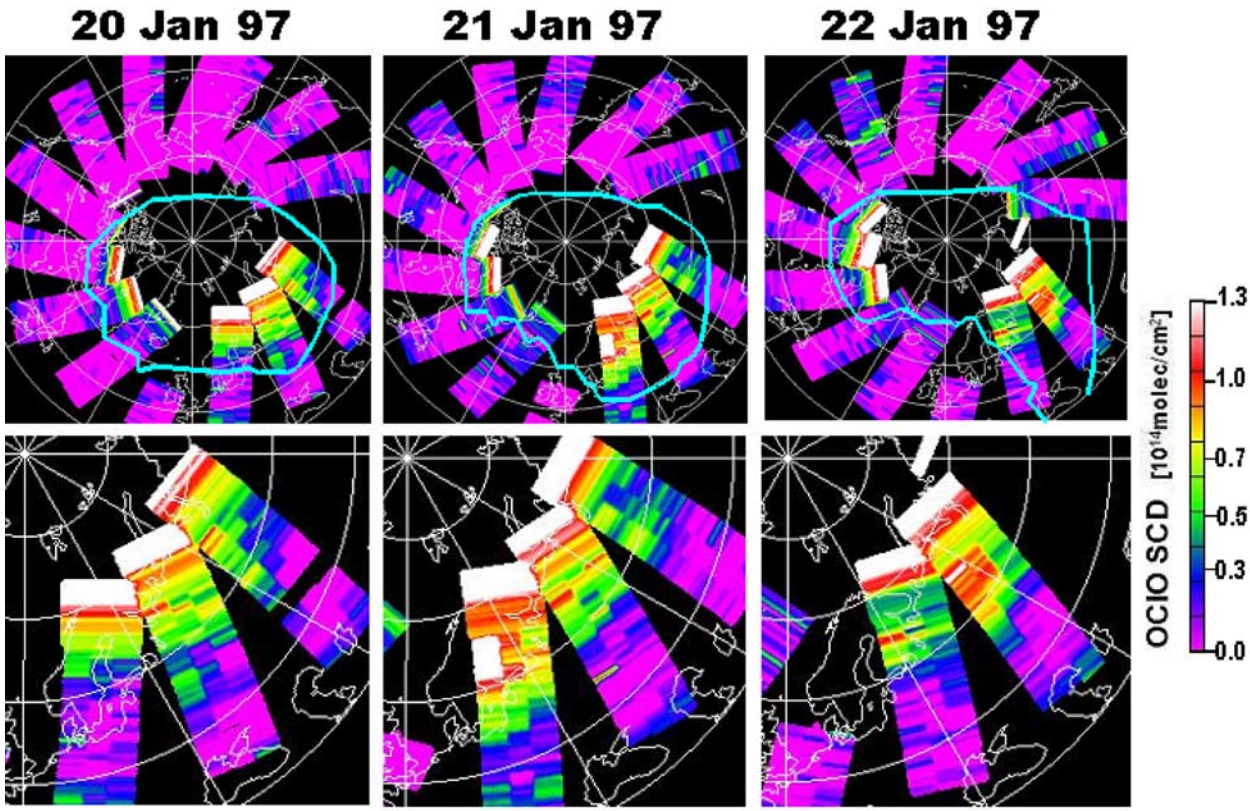

Figure 4. Maps of OClO Slant Column Densities (SCDs) derived from GOME measurements for 20 to 22 January 1997. North pole at center of the map; all orbits of the GOME measurements are shown. The solar zenith angle (SZA) ranges from 66 to 92 degrees from south to north. Owing to the polar night, trace gases cannot be observed at SZAs > 95° by GOME. There is a gradual decrease of the SCDs from north to south due to the increasing OClO photolysis and decreasing air mass factor (AMF) for lower SZA. On 21 January, a substantial increase in the slant column densities (SCDs) of OClO is seen in the lee of the Scandinavian mountain ridge.

[27] On 21 January, a substantial increase in the OClO SCDs from approximately 0.6 * 10^{14} on 20 January to 1.3 * 10^{14} (molec/cm^2) is observed above mid Scandinavia, clearly south of the already activated area inside the vortex core. Such a rapid increase of OClO in a localized area is quite unusual in all GOME measurements, especially at these relatively small solar zenith angles of 75° to 85°. As chlorine activation takes place on PSC particles, an increase in the OClO SCDs is an indication for a decrease in temperatures (or for a transport of already activated air). However, the synoptic scale temperatures in the considered region differ only marginally between 20 and 21 January [*Dörnbrack et al.*, 2001] (see also Figures 3a and 3b), and do not explain the observed increase in chlorine activation.

[28] Also, a transport of already activated air masses to the considered region can be excluded as an explanation for the increase of the OClO SCDs. Figure 5 shows synoptic-scale trajectory calculations for parcels arriving and starting at the 30 and 50 hPa levels (2.5 days back and forward trajectories) based on the code LAGRANTO [*Wernli and Davis*, 1997] and using 6 hourly ECMWF operational analyses. For parcels at 30 hPa (approximately 22 km altitude) temperatures fall below the PSC threshold (T_{NAT} = 192 K) already on 20 January, indicating that heterogeneous processing probably occurred on the synoptic scale. At the 50 hPa level (approximately 19 km altitude), the air parcels did not encounter temperatures below the PSC threshold (T_{NAT} = 195 K) before passing the Scandinavian mountain ridge.

[29] At any pressure level, temperatures below the threshold for ice formation (PSC type II) are encountered only on the mesoscale (see Figure 3c). Comparing with Figure 4, it can be seen that the GOME measurements between northern Scandinavia and the east coast of Greenland, where the air parcels originated on 20 January (based on calculations for the 30, 40 and 50 hPa level), show only weak chlorine activation in the most northern parts of the orbit (the increase of the OClO SCDs and related VCDs as a function of latitude and solar zenith angle is shown in Figure 6 and discussed in detail in section 5.2).

[30] Comparing the GOME OClO map of 21 January with the mesoscale temperature field in Figure 3c, one finds that the location of the increase in the chlorine activation level agrees very well with the location of the simulated stratospheric temperature anomaly. Due to the spatial and temporal coherence, the abrupt rise in the OClO SCDs on 21 January can be attributed to chlorine activation on PSCs formed by adiabatic cooling in mountain waves, for which

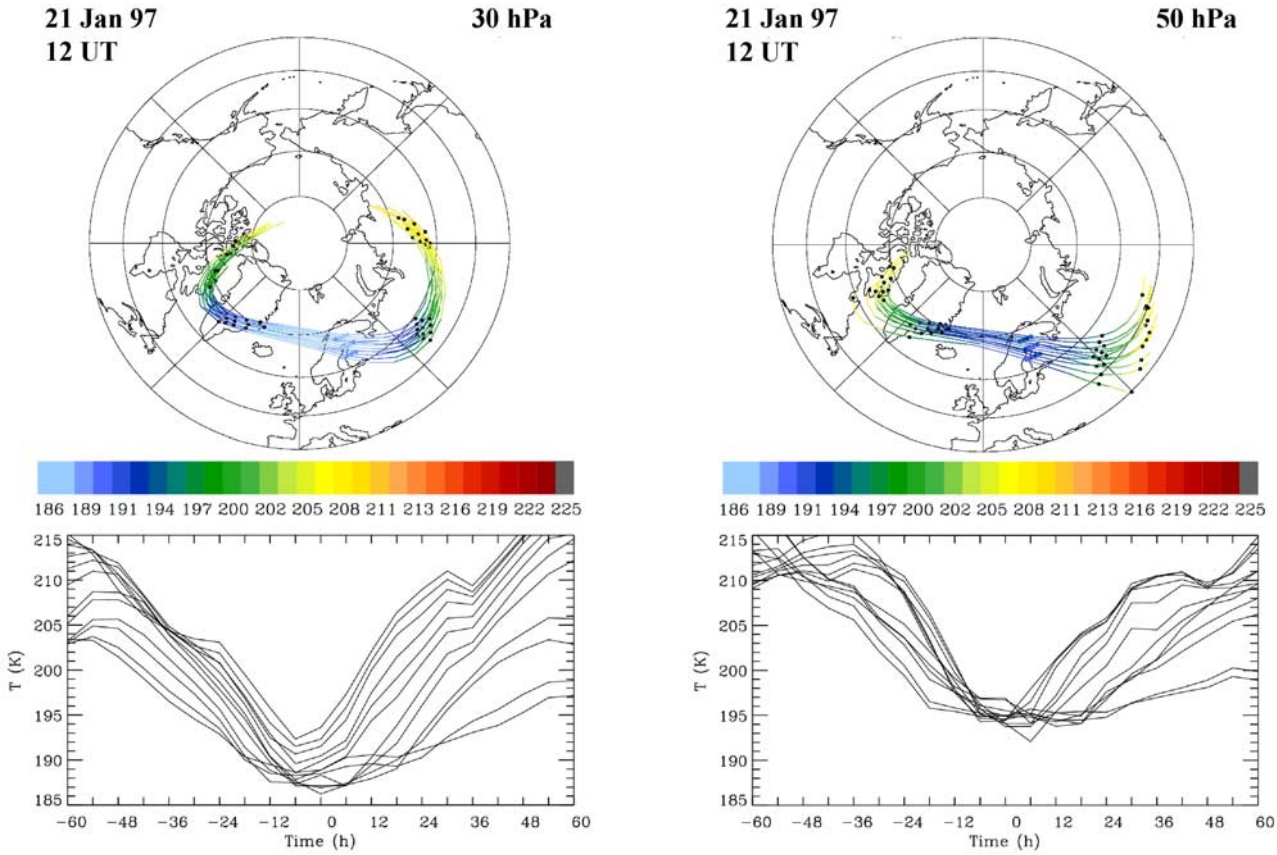

Figure 5. Backward and forward trajectories at the 30 and 50 hPa level for the air parcel for which the rapid increase of the OClO SCDs was observed above the Gulf of Bothnia on 21 January 1997. Also shown is the temporal evolution of the temperature for the respective trajectories.

the activity was reported to be strongest on that day. This is supported by the fact that similar increases in the GOME OClO observations for the same region are also correlated with strong mountain wave activity (for example 30/31 January 1996 and 25–27 January 2000).

[31] Of course, it is not possible from the GOME measurements alone to separate increases in the OClO SCDs caused by decreases of the synoptic-scale temperatures from the effect of the mesoscale mountain waves. However, since minimum synoptic-scale temperatures inside the vortex above northern Scandinavia have been varying only slightly from 18–22 January [*Dörnbrack et al.*, 2001], see also Figure 3, and temperatures below T_{NAT} were encountered only for the lowest pressure levels (corresponding to low number densities) it is reasonable to assume, that the major contribution to the observed increase of the OClO SCDs arises from the strong mountain wave activity. In agreement, *Dörnbrack et al.* [2001] have shown, on the basis of model calculations, that the mass flux of air being heterogeneously processed is increased on the mesoscale, especially during the large-amplitude mountain wave event on 21–22 January 1997.

[32] One day later, on 22 January, the activated air masses have been advected eastward (see Figure 4) with an apparent speed of approximately 10 ms^{-1}, in good agreement with ECMWF forward trajectories starting above the Gulf of Bothnia and arriving over northern Russia (see Figure 5). The air activated by the mesoscale stratospheric temperature anomalies is localized and can be clearly distinguished from activated air masses with different origin further north inside the polar vortex. While the spatial extension of this mountain wave activated air appears to have increased, especially in the west-east direction, maximum values of OClO decreased at the same time (from OClO SCDs above $1.3 * 10^{14}$ on 21 January to values around $1.0 * 10^{14}$ on 22 January), indicating that horizontal expansion of the activated air masses took place. However, on both days, the spatial extension of the mesoscale activated air masses is not fully covered by the GOME orbits. Instead, the orbits appear to miss some activation on the western part, which leads to an underestimation of the total area being heterogeneously processed (see section 6).

[33] Additionally, GOME measured a small spot of enhanced OClO SCDs above Finland east of the Gulf of Bothnia on 22 January. This increase in OClO is in good agreement with PSC observations extending from 20 to 26 km altitude by the ground-based lidar at Sodankylä, during the night of 21 January [*Stein et al.*, 1999] and with record low stratospheric temperatures measured by a regular radiosounding at the same location [*Dörnbrack et al.*, 1999]. Again, adiabatic cooling in large-amplitude mountain waves determined the local temperature distribution [*Dörnbrack et al.*, 1999].

[34] After 23 January, the region of mesoscale activated air is not distinguishable in the GOME OClO maps from usual activation on the synoptic scale. It probably has been

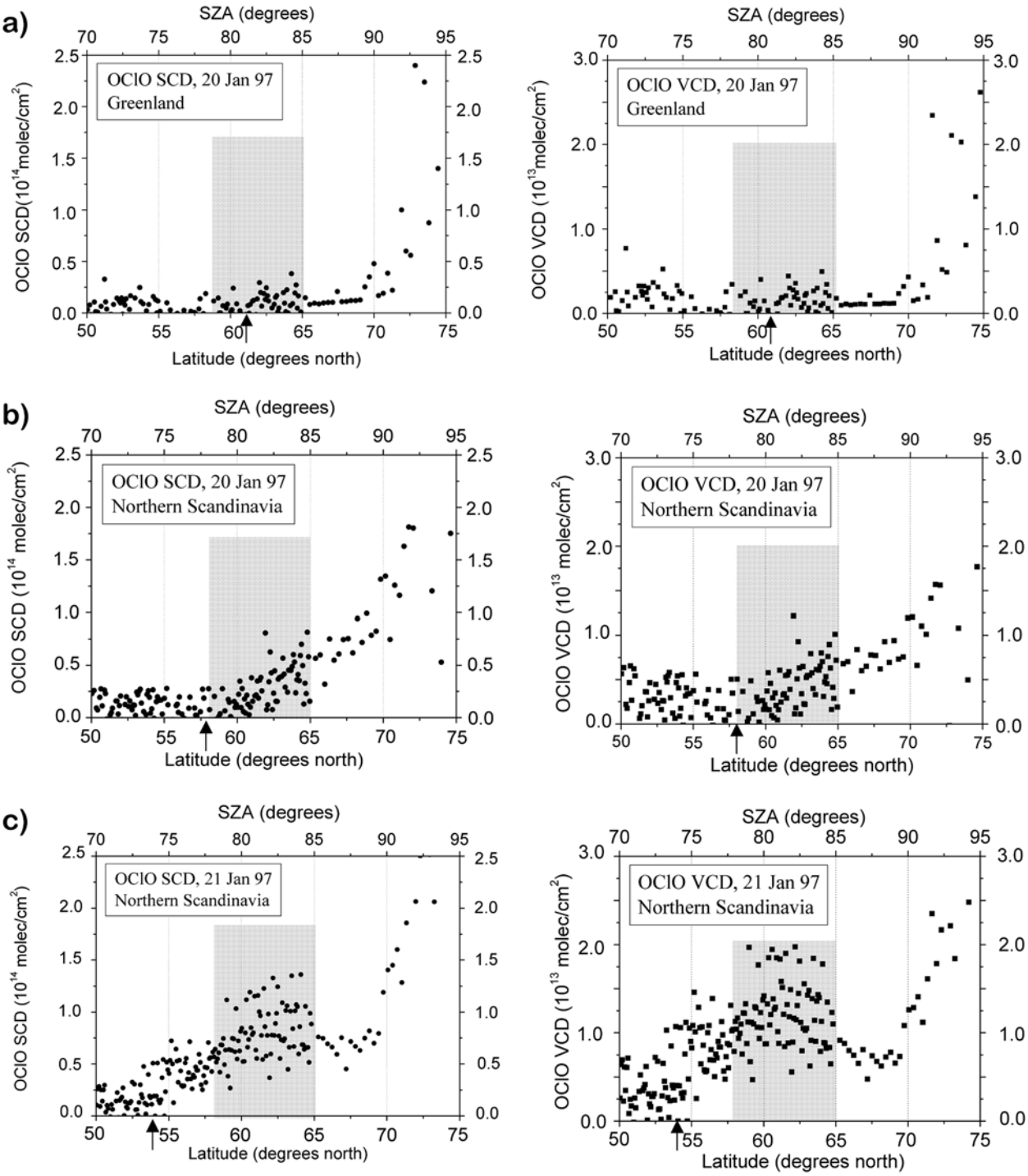

Figure 6. GOME OClO SCDs and related VCDs as a function of the solar zenith angle (SZA) and latitude. VCDs were derived with the corresponding AMFs calculated by AMFTRAN for a gaussian profile of the OClO mixing ratio, maximum at 19 km, full width half maximum of 8 km, see also Figure 1. The arrow at the latitude axis indicates the vortex edge at the 475 K level. (a) For the sum of the two orbits above Greenland on 20 January 1997. (b) For the orbit above northern Scandinavia on 20 January 1997. (c) For the orbit above northern Scandinavia on 21 January 1997.

mixed with air inside the vortex (see trajectories in Figure 5), or has been partly deactivated by reaction of ClO with NO_2 to $ClONO_2$. Trajectory calculations shown in Figure 5 reveal that the air column with enhanced OClO split after 22 January: At the 30 hPa level, the activated air masses move into the polar vortex, while they move further south at the 50 hPa level. This split of the air column also leads to a reduction of the OClO SCDs observed, even if the concen-

tration of OClO at the respective pressure levels remained constant.

5. Quantifying the Increase in Chlorine Activation

[35] Although there are several model simulations of mountain wave-induced chlorine activation [*Carslaw et al.*, 1998, 1999; *Rivière et al.*, 2000], no measurements have been reported so far detailing the extent of chlorine activation by mesoscale mountain waves. Since the synoptic-scale temperature remained almost constant [*Dörnbrack et al.*, 2001], see also Figure 3, and the relevant air mass showed only little level of activation before, the GOME observations of the OClO increase above northern Scandinavia on 21 January 1997 constitute an optimal opportunity for quantifying the chlorine activation by mountain wave-induced PSCs. For that purpose, the OClO SCDs measured by GOME are converted to VCDs. By employing a mesoscale temperature profile at the location of the measurement, the vertical column is then divided into OClO concentrations at the respective altitude levels. Utilizing the JPL 2002 recommendation for the rate constant of the formation reaction for OClO [*Sander et al.*, 2003], this leads to an estimation of the vertical ClO mixing ratio profile.

5.1. OClO as Indicator of Chlorine Activation

[36] Although OClO is not a good quantitative indicator of chlorine activation for large solar zenith angles ($\theta > 92°$) [*Sessler et al.*, 1995], there is general agreement that the concentration of OClO depends nearly linearly on the concentration of ClO and BrO for $\theta < 90°$ [*Schiller and Wahner*, 1996; *Sessler et al.*, 1996; *Tornkvist et al.*, 2002]. OClO is almost entirely formed by one product channel of the reaction between ClO and BrO [*Sander and Friedl*, 1989; *Toumi*, 1994], which forms a null-cycle regarding ozone destruction:

$$\mathrm{ClO} + \mathrm{BrO} \rightarrow \mathrm{OClO} + \mathrm{Br} \qquad (4)$$

The major loss mechanism for stratospheric OClO is its rapid photolysis:

$$\mathrm{OClO} + h\nu \rightarrow \mathrm{ClO} + \mathrm{O} \qquad (\lambda < 480\ \mathrm{nm}) \qquad (5)$$

The formation reaction (equation (4)) and the photolysis of OClO (equation (5)) lead to a quickly attained balance between ClO and OClO. Assuming a steady state, the concentration of OClO at daytime is given by [*Solomon et al.*, 1990; *Schiller and Wahner*, 1996]:

$$[\mathrm{OClO}] \approx k[\mathrm{ClO}][\mathrm{BrO}]/J(\mathrm{OClO}) \qquad (6)$$

In the above equation, the square brackets represent the concentration of the molecules, k is the rate constant for the formation reaction (equation (4)), and J(OClO) the photolysis frequency of OClO (see Figure 2). This steady state assumption and therefore the linearity between the concentrations of ClO and OClO is valid only for low SZAs ($\theta < 90°$). For higher SZAs (especially above 92°) bromine chloride (BrCl), a product formed in another channel of the ClO + BrO reaction

$$\mathrm{ClO} + \mathrm{BrO} \rightarrow \mathrm{BrCl} + \mathrm{O_2} \qquad (7)$$

becomes an important reservoir and the production of OClO via equation (4) is limited by the availability of BrO [*Sessler et al.*, 1995; *Schiller and Wahner*, 1996].

5.2. Calculation of the OClO VCDs

[37] Since the increases in the OClO SCDs measured by GOME took place in regions with relatively low SZAs ($75° < \theta < 85°$), the air mass factor (AMF) does not depend strongly on the vertical profile of OClO (see Figure 1), and the SCDs can be converted into VCDs by equation (3) with only little uncertainty. Figure 6 shows the SCDs and corresponding VCDs for the orbit above northern Scandinavia on 21 January, and for the sum of the two orbits above Greenland on 20 January, where the air parcel originated on that day (see section 4). For comparison, the SCDs and VCDs for the orbit above northern Scandinavia on 20 January (the same location, where the rapid increase of the OClO SCDs occurrs on 21 January) are also shown.

[38] An ideal approach to determine the mountain wave-induced increase in chlorine activation would be to compare the OClO column densities of the same air mass for both days by consulting the related trajectories. GOME measurements cover the place of the origin of the air mass above Greenland (see Figures 4 and 5), thereby enabling us to quantify the increase of the OClO VCDs. However, there is the complication that the related trajectories are different for each height level (see Figure 5): For the 50 hPa level (approximately 19 km altitude), the trajectory calculations reveal that the considered air mass emanated from above east Greenland on 20 January. On the other hand, trajectories for the 30 hPa level started above the mid of Greenland. These locations correspond to different GOME orbits (compare Figure 4), which makes it impossible to attribute the observed increase in the VCDs to an increase between a single pair of GOME orbits.

[39] Therefore we decided to take the sum of the OClO SCDs and VCDs of the two orbits above Greenland on 20 January (Figure 6a). The GOME OClO SCDs for 20 January above Greenland are significantly lower than the ones above northern Scandinavia (Figure 6b, see also Figure 4), even when the sum of the two Greenland orbits is taken: While the orbits above Greenland show almost no chlorine activation at the location of the air mass origin (OClO SCDs are around $0.3 * 10^{14}$ molec/cm^2), the orbit above northern Scandinavia features OClO SCDs around 0.5 to $0.7 * 10^{14}$ molec/cm^2. This indicates that, due to temperatures below T_{NAT} on the synoptic scale (see Figure 3a), air masses above northern Scandinavia were moderately activated on 20 January.

[40] As already mentioned (see section 4), the trajectories in Figure 5 reveal that, for the air parcel being heterogeneously processed by the mountain wave event on 21 January, some activation probably occurred already before passing the Scandinavian mountain ridge on the synoptic scale, especially at the low pressure levels ($p \leq 30$ hPa). In order to account for this activation on the synoptic scale and not to overestimate the mountain wave induced chlorine

activation, the following calculations investigate the increase appearing in the orbits above northern Scandinavia between 20 and 21 January. For comparison, the increase relative to the sum of the two orbits above Greenland is given in brackets. Both figures may serve as an upper and lower limit for the mountain wave induced increase in chlorine activation in the investigated air mass.

[41] Owing to the increase of the AMF, all SCDs for 20 and 21 January in Figure 6 show a gradual increase toward higher SZAs. On 21 January, an unusual rise of the SCDs above northern Scandinavia is seen at the location of the mountain wave-induced temperature anomaly (see Figure 6c). This rapid increase is seen more clearly in the related VCDs, which do not increase due to the increase of the AMF. A comparison of the OClO VCDs above northern Scandinavia on 20 January with the ones on 21 January shows a significant enhancement extending from 53°N to 65°N (73° < SZA < 85°). The most pronounced increase from approximately 0.7 (0.5) to 1.6 * 10^{13} molec/cm^2 is found for solar zenith angles between 78° and 84° (58°N to 64°N), indicating an increase in chlorine activation by a factor of 2 to 3 for the respective vertical columns. While this represents the increase of the average values for the latitude range stated, some GOME pixels, at an SZA of 83°, show an increase of the OClO VCDs from 0.8 (0.5) to above 1.9 * 10^{13} molec/cm^2, which implies significant activation of chlorine species over a wide altitude range.

[42] In the following section we investigate the increase of the OClO VCDs observed near 64°N/22°E at an SZA of 83° from 0.8 (0.5) * 10^{13} molec/cm^2 on 20 January to 1.8 * 10^{13} molec/cm^2 on 21 January. By applying different vertical OClO and ClO profiles, which are derived from the mesoscale temperature profile collocated with the observed OClO VCD, we give an estimate for the related increase of the mixing ratios of OClO and ClO.

5.3. Estimation of Vertical Profiles for the OClO and ClO Mixing Ratio

[43] One limitation of a nadir DOAS measurement is that it is only sensitive to slant column densities. By taking into account radiative transfer calculations, the related vertical column densities can be derived. Information about the vertical concentration profile of the considered absorber can be achieved only with the use of additional measurements or by making assumptions about the relative profile shape. The magnitude of the concentration profile then results by constraining the VCD, which results from a vertical integration of the concentration profile, to the observed VCD. For OClO, often a gaussian profile for the mixing ratio is assumed that is centered at a height of 19 km and has a full width at half maximum (FWHM) of 8 km, in reasonable agreement with vertical profiles measured by ballon-borne spectrometers during sunset at SZAs between 85 and 96 degrees [*Pommerau and Piquard*, 1994; *Fitzenberger*, 2001].

[44] In this study, we assume various profiles in order to investigate how the observed increase of the OClO VCDs can be attributed to an increase in the mixing ratio of OClO at the different altitude levels. Since, for low SZAs, the steady state assumption (equation (6)) holds, meaning that [OClO] is linear to [ClO], the corresponding mixing ratios of ClO can then be calculated. For all calculations, we apply the temperature and pressure profile derived from the mesoscale calculations for the location of the high OClO SCDs measured by GOME near 64°N/22°E on 21 January. Furthermore, we assume a constant mixing ratio for BrO of 15 pptv and consider the height-dependence of the photolysis rate of OClO. The rate constant for the formation reaction of OClO (equation (4)) is taken from the JPL 2002 recommendation [*Sander et al.*, 2003]. The uncertainties of the calculations and the underlying assumptions as well as the sensitivity of the results on parameters not observed by GOME are discussed in section 6.

[45] The motivation for the different profile shapes is given by the dependence of chlorine activation on the formation of PSCs, i.e., we assume that high levels of chlorine activation are to be found for altitudes where temperatures drop below the threshold for formation of PSCs. In Figure 7, a cross-section of the simulated mesoscale temperatures along a trajectory downstream of the Scandiavian mountain ridge including the location of the OClO VCD of 1.8 * 10^{13} molec/cm^2 on January 21 near 64°N/22°E is plotted. It can be seen that minimum temperatures of 187 K are found at the 520 K level, which is below T_{NAT}, the threshold for formation of PSC type Ia, already before the air parcels reach the Scandinavian mountain ridge. However, temperatures below T_{frost}, the threshold for formation of PSC type II, are encountered only downstream of this high mountain barrier. In addition, the vertical extension of the altitude for which formation of PSCs and hence chlorine activation is possible, is significantly enhanced by the mountain wave-induced temperature anomaly.

[46] The altitude region with possible PSC formation can be seen more easily in Figure 8. It shows the range of temperatures that the air masses encountered traveling downstream of the Scandiavian mountain ridge up to the location of the observed maximum VCD of OClO in comparison to the PSC formation threshold temperatures. T_{NAT} and T_{frost} were calculated according to *Hanson and Mauersberger* [1988] with the assumption of constant mixing ratios for nitric acid and water vapor (HNO_3 = 10 ppbv and H_2O = 5 ppmv). According to this estimate, formation of PSC type Ia (NAT) was possible in an altitude range from 15 to 28 km, while temperatures below T_{frost} occur in the range from 21 to 24 km.

[47] These calculations are in good agreement with Lidar measurements above Sodankyla during the nights of 21 and 22 January [*Stein et al.*, 1999], where PSCs were observed from 20 to 26 km, and PSCs type II were observed from 21.5 to 22.5 km. In addition, the mesoscale temperature profile calculated by MM5 for the 21 January 1997 has been shown to be in very good agreement with measurements from ozone sondes [*Dörnbrack et al.*, 1999]. In sections 5.3.1 to 5.3.3 we assume three different vertical profile shapes for the ClO mixing ratio, based on the estimate of possible PSC formation derived from the mesoscale temperature profile. First, the altitude range of temperatures below T_{NAT} is considered by assuming a box profile for the ClO mixing ratio (see section 5.3.1).

[48] As the probability of PSC formation increases for lower temperatures, higher ClO and OClO concentrations are to be expected for altitude levels with lower temperatures. A rough approximation to the probability for chlo-

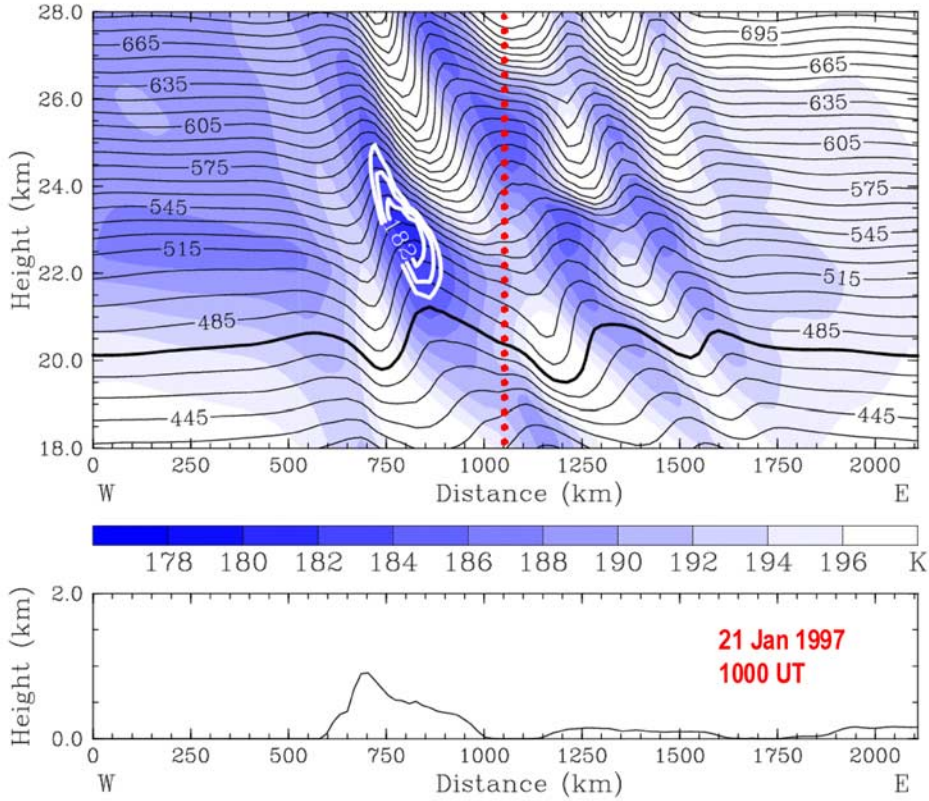

Figure 7. Temperature T < 196 K (color shaded; K) and potential temperature Θ (solid black lines, ΔΘ = 10 K) on 21 January 1997, 1000 UT (close to the time of the GOME measurement) along the vertical west-east section marked by the red line in Figure 3b. The location of the maximum OClO VCD, for which the vertical profile of the chlorine activation is calculated, is indicated by the red dotted line. Temperatures below T_{frost} are indicated by the white shaded contours. The height of the model orography is plotted below the vertical section. Numerical results are from the outer domain of the mesoscale model (Δx = 27 km).

rine activation or formation of PSCs as a function of altitude is given in Figure 9. It shows the difference of the simulated temperatures to the PSC type Ia formation temperature (T_{NAT}). This temperature difference profile can be well described by a gaussian function with the maximum at a height of 21 km and a full width at half maximum of 8 km. In section 5.3.2, we assume this gaussian fit to the temperature profile as the vertical profile for the ClO mixing ratio. In section 5.3.3, we assume that the ClO mixing ratio profile has exactly the same shape as the temperature difference profile derived from the simulated mesoscale temperature profile.

[49] We want to point out here that the OClO and ClO mixing ratio profiles discussed in the following are not measured by GOME but derived from assumptions about the relative profile shape. Since there are no other measurements detailing the extent of mountain wave induced chlorine activation, we want to give a rough estimate of the increase in quantities that are more familiar than OClO column densities. Of course, there are many uncertainties in the necessary calculations and further uncertainties arise due to the assumptions made (see section 6). However, the result of a rapid increase of the OClO and ClO mixing ratios over a wide altitude range during the mountain wave event is the same for all profiles that can be assumed due to the given meteorological situation.

5.3.1. Box Profile for Mixing Ratio of ClO

[50] This box profile indicates, which ClO mixing ratios are consistent with the observed GOME OClO VCDs, when no specific profile is assumed. At the same time, this profile may represent the threshold character of the processes involved in chlorine activation. We assume that activation of chlorine takes place when temperature drops below the threshold for formation of PSCs and neglect the temperature dependence of the reactions involved. This results in a constant ClO mixing ratio for altitudes where PSC formation was possible on 21 January (15 to 28 km, see Figure 8). Using the steady state assumption (equation (6)), this ClO box-profile can be constrained to the GOME OClO measurements by changing its maximum mixing ratio until the resulting OClO VCD matches the OClO VCD measured by GOME. For 21 January, the OClO VCD of 1.8 * 10^{13} molec/cm^2 measured by GOME corresponds to a constant ClO mixing ratio of 1.3 ppbv. The same box profile applied to the GOME OClO VCD of 0.8 (0.5) * 10^{13} molec/cm^2 measured on 20 January, results in a ClO mixing ratio of 0.6 (0.4) ppbv. This implies that for the total column, the level of activation increased by a factor

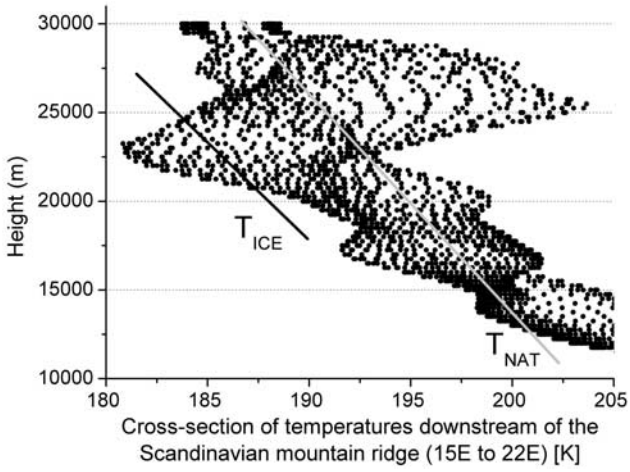

Figure 8. Range of temperatures encountered by air parcels 400 km upstream of the location of the high OClO VCDs on 21 January, 1000 UT, as calculated by MM5 for the west-east section in Figure 7 (see also the red line in Figure 3b), approximately from 15°E to 22°E (from the mountain ridge to the location of the GOME measurement). In comparison, the threshold temperatures for the formation of PSC type 1 (T_{NAT}, blue line) and PSC type 2 (T_{ICE}, red line) at the respective height levels are shown. The PSC formation temperatures were calculated according to *Hanson and Mauersberger* [1988], assuming 10 ppbv HNO_3 and 5 ppmv H_2O.

of 2.2 (3.4); the values in brackets indicate the increase relative to the sum of the two orbits above Greenland (see section 5.2).

5.3.2. Gaussian Profile of ClO Mixing Ratio, Derived From the Mesoscale Temperature Profile

[51] The next two profiles account for the temperature dependence of the heterogeneous chlorine activation reactions by linearly increasing the volume mixing ratio of ClO for altitudes with temperatures below T_{NAT}. First, we adopt the gaussian function to the temperature profile shown in Figure 9 for the vertical profile of the ClO mixing ratio and constrain it to the GOME OClO measurements as described above.

[52] In particular, this allows us to calculate the mixing ratios of OClO and ClO at the 30 and 50 hPa level for the air parcel for which the high OClO VCDs were measured by GOME on 21 January. The observed VCD of OClO on 21 January of 1.8 * 10^{13} molec/cm^2 near 64°N/22°E corresponds to an OClO concentration of 6.3 * 10^6 molec/cm^3 at 30 hPa (22.3 km) and 1.7 * 10^7 molec/cm^3 at 50 hPa (19.5 km) (mixing ratios: 5.5 and 9.1 pptv respectively). Following the steady state assumption (equation (6)), these OClO concentrations correspond to mixing ratios for ClO of 1.7 ppbv at 30 hPa and 1.6 ppbv at 50 hPa.

[53] For 20 January, we assumed the same gaussian profile for ClO, which is constrained to the GOME OClO measurements in the described way. On that day the OClO VCD measured by GOME at 64°N/22°E (SZA of 83°) was 0.8 * 10^{13} molec/cm^2, resulting in substantially lower mixing ratios for ClO (0.75 ppbv at 30 hPa and 0.7 ppbv at 50 hPa) and OClO (2.5 pptv at 30 hPa and 4.1 pptv at 50 hPa). The vertical profile for the OClO mixing ratio resulting from the calculation sketched above for 21 January is shown in Figure 10.

5.3.3. Profile of ClO Mixing Ratio Directly Scaled to Mesoscale Temperature Profile

[54] The gaussian fit to the simulated mesoscale temperatures overestimates the temperature difference to T_{NAT} below 22 km, where $\Delta T = T_{NAT} - T$ shows a rapid rapid decrease (see Figure 9). This probably leads to an overestimation of the mountain wave-induced chlorine activation at these altitudes. At the same time, the gaussian fit underestimates the temperature-difference to T_{NAT} (and consequently the induced chlorine activation) for heights between

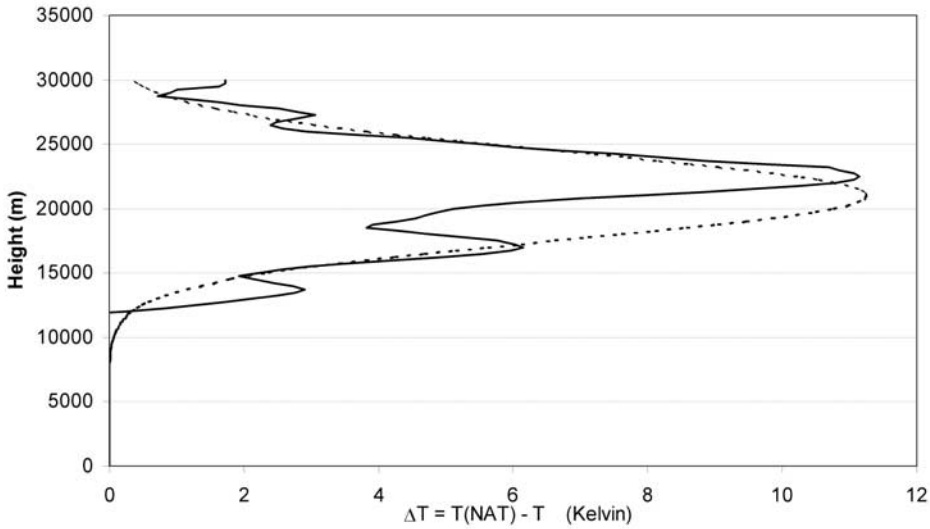

Figure 9. Temperatures below T_{NAT} encountered by air parcels 400 km upstream of the location of the maximum OClO VCD near 64°N/22°E on 21 January as an estimate for the probability of chlorine activation. Also shown is a gaussian fit to the curve with the maximum at 21 km and a full width at half maximum of 8 km.

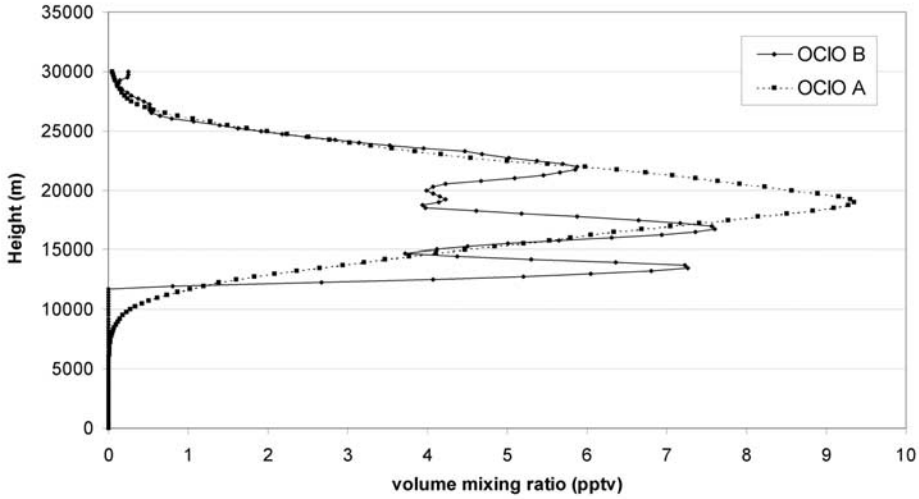

Figure 10. Vertical profiles of the OClO mixing ratio on 21 January 1997, according to the temperature difference profile obtained from the mesoscale simulations (see Figure 9) and scaled to the GOME observations of the OClO SCDs. Calculations were performed using the mesoscale temperature and pressure profiles at the location of the GOME measurement and applying the JPL 2002 recommendation [*Sander et al.*, 2003] for the rate constant of the formation reaction of OClO (details see text). 'OClO A': for the ClO volume mixing ratio profile scaled by the gaussian fit to the temperature difference profile with maximum at 21 km and full width at half maximum of 8 km. 'OClO B': for the ClO volume mixing ratio profile scaled directly by the difference of the simulated mesoscale temperatures to T_{NAT} (see Figure 11).

13 and 15 km. Since these altitude levels have higher number densities, possible chlorine activation at these heights will lead to high concentrations of OClO and thus could represent a significant part of the observed OClO VCD, even when the mixing ratio of OClO (or ClO) is lower than for higher altitudes.

[55] The possible chlorine activation in the high pressure regions (low altitudes) is better accounted for, if we adopt the difference of the mesoscale temperatures to the threshold for formation of PSC type Ia (T_{NAT}), shown in Figure 9, for the vertical profile of the ClO mixing ratio. The resulting profile (see Figure 11) shows the same wave-like structure as the mesoscale temperatures, with minima and maxima alternating with a period of approximately 4–5 km. The derived OClO profile depicts three peaks with nearly the same magnitude (see Figure 10), arising mainly from a weighting of the ClO profile with the height dependent photolysis rate of OClO.

[56] Figure 11 depicts the mixing ratios for ClO and ClO_x(=ClO + ClOOCl × 2), resulting at an SZA of 83° at the respective pressure levels. The ClO mixing ratios were calculated for three different BrO profiles of constant mixing ratio: 12, 15, and 18 pptv. The ClO_x values were calculated for two scenarios: (1) according to the JPL 2002 recommendation [*Sander et al.*, 2003], and (2) by increasing J(ClOOCl) by a factor of 1.3, as suggested by *Stimpfle et al.* [2004]. Compared to the gaussian fit (see section 5.3.2), mixing ratios for ClO at the height of 19.5 km (≈50 hPa) are significantly reduced (from 1.6 to 0.7 ppbv). However, mixing ratios at the 30 hPa level (≈22 km) remain nearly unchanged (0.8 compared to 0.7 ppbv on 20 January, and 1.75 compared to 1.7 ppbv on 21 January). The resulting mixing ratios for ClO_x are below the total Cl_y for all height levels [*Schmidt et al.*, 1994; *Engel et al.*, 2002], but reveal that almost complete activation of chlorine occurred, especially in the mountain wave induced temperature minima.

[57] The shape and magnitude of the derived ClO profile is in good agreement with observations: While ground and space based microwave measurements show a gaussian shape vertical profile with peak mixing ratios around 2 ppbv [*Solomon et al.*, 2002; *Santee et al.*, 2003], high resolution in situ measurements reveal that the ClO mixing ratio profile can consist of multiple peaks [*Pierson et al.*, 1999; *Vogel et al.*, 2003], depending on the temperature profile which enabled the heterogeneous processing of chlorine species in PSCs.

6. Discussion: Implications and Uncertainties

6.1. Implications for Stratospheric Chlorine Activation in the Arctic

[58] The GOME OClO observations above northern Scandinavia during 20–22 January 1997 provide the first measurement of mountain wave induced chlorine activation. The vertical column densities of OClO increase from 0.8 (0.5) * 10^{13} to 1.8 * 10^{13} molec/cm^2 implying that, for the total column, the level of chlorine activation increased by a factor of 2.2 (3.4). This increase in chlorine activation must have occurred in an altitude region where formation of PSCs was possible. By applying mesoscale calculations for the temperature and pressure profile at the location of the GOME measurements we attribute the increase of the OClO VCD to increases of the OClO and ClO mixing ratios. It is found that the observed OClO VCD corresponds to a vertical range of the activated air mass from approximately 17 to 27 km altitude (mixing ratios for ClO greater than

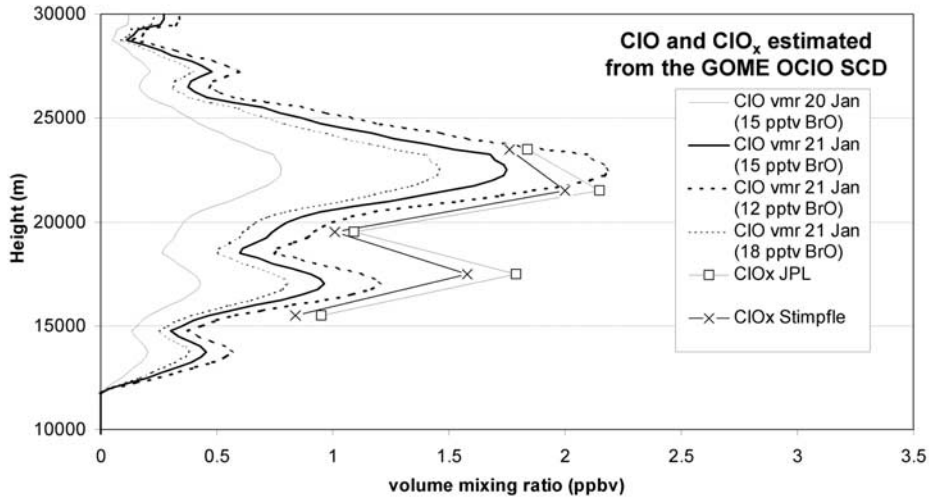

Figure 11. Vertical profiles of the ClO mixing ratio on 20 and 21 January 1997, estimated from the GOME observations of the OClO SCDs by applying the temperature difference profile ($\Delta T = T_{NAT} - T$) obtained from the mesoscale simulations (see Figure 9). The ClO mixing ratio profile for 21 January is plotted for three different BrO profiles of constant mixing ratio: 12, 15, and 18 pptv; for 20 January only the ClO profile resulting for 15 pptv BrO is plotted. Details of the calculations based on the steady state assumption are described in the text. Also shown is the resulting mixing ratio for ClO_x(=ClO + ClOOCl × 2) for 15 pptv BrO for 21 January, applying either the JPL 2002 recommendation [*Sander et al.*, 2003], or increasing J(ClOOCl) by the factor 1.3 as suggested by *Stimpfle et al.* [2004].

0.8 ppbv). As ice PSCs could be present only in the range from 21 to 24 km, this indicates that significant activation of chlorine species took place not only on the ice particles (PSC type II) but also on PSC type I (NAT). On the other hand, if we assume that the observed OClO VCD of 1.8 * 10^{13} molec/cm^2 is confined to altitudes between 21 and 24 km, unrealistically high ClO mixing ratios are derived, for which the resulting ClO_x values exceed the total availabe inorganic chlorine.

[59] The spatial extension of the air masses, which have been chlorine activated in consequence of the mountain wave cooling, can be calculated straight forward: With a number of at least 60 GOME pixels that show an increase of the VCDs from below 0.6 to above 1.0 * 10^{13} molec/cm^2 and a ground pixel size of 40 * 320 km^2 this corresponds to an area of approximately 750.000 km^2. Compared to the total size of the polar vortex of 23.0 * 10^6 km^2 at that day, this indicates that approximately 3% of the area of the polar vortex has been heterogeneously processed by the mountain wave event. However, as already mentioned in section 4, the GOME orbits appear to miss some activated air masses to the west of the orbits with high OClO SCDs. Therefore it is likely that the actual area of the air masses that have been activated by adiabatic cooling due to the mountain wave event is still larger. For comparison, the area that contained NAT particels due to the mountain wave event on 11 January 1995 was calculated by *Carslaw et al.* [1999] to 600.000 km^2 at the 475 K level.

[60] For all vertical profiles assumed, the deduced increase in the ClO mixing ratio from 20 to 21 January corresponds to a chlorine activation rate of above 1.0 ppbv per day at the 30 hPa level. Compared to values at the synoptic scale, these values are around 4–5 times higher [see, e.g., *Drdla and Schoeberl*, 2003; *Solomon et al.*, 2002], but are in good agreement with model studies of chlorine activation due to mesoscale mountain wave PSCs, where a difference of 0.9 to 2.1 ppbv was calculated for the ClO mixing ratio, either taking into account mountain-wave perturbations or excluding them [*Rivière et al.*, 2000]. In a similar study, *Carslaw et al.* [1998] calculated 1.6 ppbv for the mixing ratio of active chlorine in an air mass heterogeneously processed by mountain-wave-induced mesoscale PSCs, compared to 0.1 ppbv for the synoptic scale.

[61] The very high chlorine activation rate and the huge area activated in only one day (or, if we consider the windspeed, in only four hours), confirms the high efficiency of stratospheric mountain waves in activating chlorine species: While the cold phases of the waves remain above the same place nearly stationary, fast airflow through these cold phases leads to heterogeneous processing of large air masses.

[62] *Carslaw et al.* [1998] have shown that chlorine activation induced by mesoscale mountain wave PSCs leads to additional depletion of ozone. The observed mountain wave-induced enhancements of OClO discussed in our article take place in sunlit regions (75° < SZA < 85°). Therefore the activation of chlorine immediately leads to effective ozone depletion by the catalytic cycles. Further destruction of ozone occurs when the activated air mass stays in or returns to areas exposed to sunlight, or if it remains activated until the end of the polar night. However, some of the air masses that are activated by mesoscale mountain wave events might also get activated on the synoptic scale until polar spring.

[63] Thus chemical ozone loss will be increased compared to activation on the synoptic scale. Model studies based on synoptic scale temperature analyses tend to underestimate chlorine activation and ozone loss in the

Arctic stratosphere [*Lutman et al.*, 1997; *Hansen et al.*, 1997; *Becker et al.*, 1998; *Woyke et al.*, 1999; *Becker et al.*, 2000a, 2000b]. The GOME OClO observations presented in this study give further reason to suggest that this discrepancy might partly be explained by chlorine activation on mesoscale mountain wave PSCs.

[64] This study focuses on the mountain wave event of 21 January 1997 because for that day, the effect of the change of the synoptic-scaled temperatures on the activation of chlorine species can be either neglected or accounted for (see above) and therefore the increase in chlorine activation due to the mountain wave-induced PSC formation can be determined. In addition, the same mountain wave event has already been studied in detail by *Dörnbrack et al.* [2001], and the mesoscale temperature profile could be used to improve the assumed profile for the ClO mixing ratio.

[65] As already mentioned, there are also other days for which mountain wave activity was reported and for which a corresponding increase of the OClO SCDs is observed in the GOME measurements. These include also mesoscale activation above the Urals and transport of chlorine activated air from the east coast of Greenland to northern Scandinavia, which have been postulated by model studies [*Carslaw et al.*, 1999].

[66] Above northern Scandinavia, the strongest increases in the GOME OClO SCDs are observed for the month of January in the cold Arctic winters (30/31 January 1996, 20–22 January 1997, 25–27 January 2000). This is in good agreement with the study by *Dörnbrack and Leutbecher* [2001] which has shown that the mountain wave activity in this region is highest for that month and that formation of PSC type II in the Arctic stratosphere is controlled by orographically induced gravity waves at cold synoptic scale 'background' temperatures. However, GOME also measures a rise in the OClO SCDs for days with only moderate mountain wave activity and also in warm Arctic winters (for example on 16 January 1997; 12 January 1998; 14 December 2001; 12–14 January 2001). In these cases, adiabatic cooling in mountain waves induces the formation of PSC type I and the activation is localized to smaller areas. For some of these days there are modelling studies on the related chlorine activation and PSC formation [*Fricke et al.*, 1997; *Wirth et al.*, 1999]. In both cases, for cold and warm Arctic winters, heterogeneous processing of chlorine due to mesoscale mountain wave PSCs leads to enhanced ozone loss, as has been shown by *Carslaw et al.* [1998].

[67] For all cold Arctic winters observed by GOME (1996–2003), an enhancement of OClO correlated to mountain wave activity, similar to the one reported in this study, occurs in January (see dates above). Likewise, for 11 January 1995, *Carslaw et al.* [1999] reported a mountain wave event above northern Scandinavia with large areal coverage, while *Dörnbrack and Leutbecher* [2001] have shown that the maximum stratospheric mountain wave activity is found in January. This is very remarkable in the context that the discrepancy between calculated and observed ozone loss in the Arctic vortex is largest in this month [*Becker et al.*, 2000a, 2000b; *Rex et al.*, 2003]. Although there must be also other reasons for the underestimation of ozone loss in cold Arctic winters [*Rex et al.*, 2003], it is certainly worth to investigate if mountain wave-induced chlorine activation can explain a part of this discrepancy.

6.2. Estimation of the Measurement Errors and Uncertainties of the Calculations

[68] Uncertainties of the GOME OClO analysis were discussed in detail by *Wagner et al.* [2001]. The precision was estimated to about ±10% for large OClO SCDs and the additional systematic errors arising from the absolute calibration of the OClO cross section are less than 8%. In the same study, the influence of the optical density of PSCs on the AMF for OClO was investigated. In particular, it was shown that PSCs have only a negligible effect on the retrieved OClO SCD.

[69] For the GOME OClO measurements presented in this study, an additional error may arise from the extraordinarily high backscatter ratio of mountain wave PSCs. Since the bulk of the OClO SCD is located below the PSCs, this could lead to an underestimation of the OClO SCD (shield effect). However, the influence of the PSCs on the retrieved OClO SCDs should be of greater importance for higher SZAs around 90° and is expected to be negligible for lower SZAs, for which the increase in chlorine activation was observed in this study. This view is supported by the very high OClO and ClO concentrations resulting from the calculations in section 5 for 21 January 1997, which indicate that a shielding by PSCs does not occur.

[70] In the conversion of the OClO SCDs to VCDs, further uncertainties arise as it depends on the AMF. As is seen in Figure 1, the calculation of the AMF for the SZAs relevant for this study ($75° < SZA < 85°$) shows only slight variation for different OClO profiles: For a gaussian profile with maximum at 19 km and a FWHM of 8 km the AMF is 7.1 at an SZA of 83°. For the same SZA and FWHM the AMF is 7.4 when the maximum is at 21 km and 6.9 when the maximum is at 18 km. Comprising the AMF for OClO at an SZA of 83° can be determined independently of the actual profile with an uncertainty less than 10% (neglecting profiles that can be excluded due to the meteorological situation). Likewise, for low SZAs, the calculation of the photolysis rate of OClO (J (OClO)) can be done with relatively low uncertainty (±5%), leading to a good approximation of the ClO/OClO relation by the steady state assumption (equation (6)).

[71] As the concentration of OClO and the deduced mixing ratio of ClO are calculated from the VCD, they depend on the vertical profile of OClO, which has to be assumed or can be estimated from the temperature profile. We investigated this uncertainty by assuming different profile shapes with different vertical extensions. For a profile, which shape was adopted from the profile of the mesoscale temperatures, we derive ClO mixing ratios that indicate almost complete activation of chlorine species. Even for a box profile extending over the whole altiude range for which PSC formation was possible (15–28 km), the ClO mixing ratio amounts to 1.3 ppbv. If, in contrast, the vertical extension is limited to a region between 21 and 24 km (approximately the altitude region where $\Delta T = T_{NAT} - T$ has the highest values), unrealistically high values result for the ClO mixing ratio. Parameters that effect the estimated vertical range of PSC-formation are the

mixing ratios of HNO_3 and H_2O. Here we assumed standard values for the polar stratosphere.

[72] The resulting mixing ratios for ClO are also influenced by the vertical profiles of the BrO mixing ratio and the mesoscale temperature. The simulated mesoscale temperature profile has been shown to match very good with measurements of an ozonesonde at Sodankylä [*Dörnbrack et al.*, 1999]. In order to investigate the sensitivity of the ClO mixing ratio on the assumed BrO profile, BrO mixing ratios were increased and decreased from the standard calculation by 20%, i.e., from 15 pptv to 12 and 18 pptv, representing the range of measured profiles [*McKinney et al.*, 1997; *Harder et al.*, 1998; *Fitzenberger*, 2001] and model calculations [*Sinnhuber et al.*, 2002]. Since steady state between OClO and its educts is assumed, the ClO mixing ratios deduced from the observed OClO VCDs are then lowered or increased by 20%, respectively.

[73] There are considerable uncertainties in the kinetics and the partitioning of the reaction between ClO and BrO [*Sander et al.*, 2003]. However, this uncertainty would only alter the absolute values of the deduced mixing ratios for ClO, the relative increase of the OClO and ClO mixing ratios as well as of the observed OClO SCDs and VCDs is unaffected.

7. Conclusions

[74] GOME observations of OClO in the northern hemisphere show a rapid increase during periods with strong mountain wave activity, confirming the importance for chlorine activation and subsequent ozone depletion that has been postulated by model calculations [*Carslaw et al.*, 1998]. For the mountain wave event above northern Scandinavia on 21 January 1997, we combined GOME OClO measurements with information on the temperature profile from mesoscale calculations, to study the effect of stratospheric mountain waves on chlorine activation in a quantitative way. The increase is found to be substantial: The OClO vertical column densities rise by a factor of about 2 (from 0.8 to 1.8 * 10^{13} molec/cm^2) at the location of the mountain wave induced temperature anomaly. This is in good agreement with model calculations of the heterogeneously processed air masses for the same mountain wave event [*Dörnbrack et al.*, 2001].

[75] In agreement with Lidar PSC observations, mesoscale calculations for the location of the GOME measurement show that, due to adiabatic cooling by the strong mountain wave activity, formation of PSCs was possible over a wide altitude range. By applying different profiles based on the mesoscale temperature profile, the increase of the OClO and ClO mixing ratios is deduced and is found to be depending only slightly on the assumed vertical profile. For a profile scaled by the difference of the simulated mesoscale temperatures to T_{NAT}, ClO mixing ratios at the 50 (30) hPa level rise from 0.3 to 0.7 ppbv (0.8 to 1.75 ppbv) due to the mountain wave event. For a box profile extending over the altiude region with possible PSC formation, ClO mixing ratios jump from 0.6 to 1.3 ppbv at all altitude levels. Thereby, the possible activation on the synoptic scale was taken into account by taking an air mass as reference that was already activated under similar synoptic conditions. If activation on the synoptic scale is also considered and the increase in chlorine activation is calculated for the same air mass, the rise of the mixing ratios is only slightly larger, implying that the major part of the air mass was heterogeneously processed on the mesoscale.

[76] This increase in ClO mixing ratios estimated from the GOME OClO measurements is in good agreement with model studies: For 21 January 1997, mesoscale meteorological simulations with the MM5 model by *Dörnbrack et al.* [2001] simulated an increase of the heterogeneously processed air masses above Scandinavia by a factor of 3, in very good agreement with the GOME observations. An increase of more than a factor of 2 in daytime ClO concentration was also found in the case study by *Rivière et al.* [2000] for the mountain wave PSC event on 25/26 February 1997. In a similar study, *Carslaw et al.* [1998] modeled almost complete conversion of the chlorine species (1.5 ppb Cl_x compared to almost no activation under synoptic-scale conditions). Furthermore, the additional area of activated air of 750.000 km^2, derived from the GOME measurements, is about 25% larger as the area calculated to contain NAT particles induced by mountain waves from the study by *Carslaw et al.* [1999].

[77] These observations confirm the importance of mountain waves for chlorine activation that is not accounted for by synoptic temperature analyses [*Carslaw et al.*, 1998]. Model calculations of ozone loss presently do not include these mesoscale processes, which therefore are one possible explanation for the underestimation of chlorine activation and ozone loss in the Arctic stratosphere [*Lutman et al.*, 1997; *Woyke et al.*, 1999; *Becker et al.*, 2000a, 2000b]. It is remarkable that this discrepancy is highest in the month of January [*Becker et al.*, 2000a, 2000b], when the activity of mountain waves has its maximum [*Dörnbrack and Leutbecher*, 2001] and thus increases in chlorine activation will be of the type reported here.

[78] **Acknowledgments.** We want to thank two anonymous referees for very constructive comments and suggestions. The financial support by HGF/ENVISAT is gratefully acknowledged. The operational meteorological analyses are provided in the framework of the ECMWF special project "Influence of nonhydrostatic mountain waves on the stratosphere above Scandinavia" by one of the authors (A.D.). We thank Heini Wernli (University of Mainz) for his trajectory code LAGRANTO. The numerical simulations were performed at the NEC SX6 supercomputer of the German Climate Research Center (DKRZ) in Hamburg, Germany. We want to thank the NILU data center in Kjeller (Norway) for providing the ECMWF analysis and the ESA center in Frascati (Italy) and the DLR center in Oberpfaffenhofen (Germany) for providing the GOME level 1 data.

References

Becker, G., et al. (1998), Ozone loss rates in the Arctic stratosphere in the winter 1991/92: Model calculations compared with Match results, *Geophys. Res. Lett.*, *25*, 4325–4328.

Becker, G., R. Müller, D. S. McKenna, M. Rex, and K. S. Carslaw (2000a), Ozone loss rates in the Arctic stratosphere in the winter 1994/1995: Model simulations underestimate results of the Match analysis, *J. Geophys. Res.*, *105*, 15,175–15,184.

Becker, G., J.-U. Grooß, D. S. McKenna, and R. Müller (2000b), Stratospheric photolysis frequencies: Impact of an improved numerical solution of the radiative transfer equation, *J. Atmos. Chem.*, *37*, 217–229.

Borrmann, S., S. Solomon, J. E. Dye, D. Baumgardner, K. K. Kelly, and K. R. Chan (1997), Heterogeneous reactions on stratospheric background aerosols, volcanic sulfuric acid droplets, and type I polar stratospheric clouds: Effects of temperature fluctuations and differences in particle phase, *J. Geophys. Res.*, *102*, 3639–3648.

Burrows, J. P., et al. (1999), The Global Ozone Monitoring Experiment (GOME): Mission concept and first scientific results, *J. Atmos. Sci.*, *56*, 151–175.

Carslaw, K. S., et al. (1998), Increased stratospheric ozone depletion due to mountain-induced atmospheric waves, *Nature*, *91*, 675–678.

Carslaw, K. S., et al. (1999), Widespread solid particle formation by mountain waves in the Arctic stratosphere, *J. Geophys. Res.*, *104*, 1827–1836.

Chipperfield, M. (1999), Multiannual simulations with a three-dimensional chemical transport model, *J. Geophys. Res.*, *104*, 1781–1805.

Coy, L., E. R. Nash, and P. A. Newman (1997), Meteorology of the polar vortex: Spring 1997, *Geophys. Res. Lett.*, *24*, 2693–2696.

Deshler, T., T. Peter, R. Müller, and P. Crutzen (1994), The lifetime of leewave-induced particles in the Arctic stratosphere: 1. Ballonborne observations, *Geophys. Res. Lett.*, *21*, 1327–1330.

Dörnbrack, A., and M. Leutbecher (2001), Relevance of mountain wave cooling for the formation of polar stratospheric clouds over Scandinavia: A 20-year climatology, *J. Geophys. Res.*, *106*, 1583–1593.

Dörnbrack, A., M. Leutbecher, R. Kivi, and E. Kyrö (1999), Mountain-wave induced record low stratospheric temperatures above northern Scandinavia, *Tellus, Ser. A*, *51*, 951–963.

Dörnbrack, A., et al. (2001), Relevance of mountain wave cooling for the formation of polar stratospheric clouds over Scandinavia: Mesoscale dynamics and observations for January 1997, *J. Geophys. Res.*, *106*, 1569–1581.

Dörnbrack, A., et al. (2002), Evidence for inertia gravity waves forming polar stratospheric clouds over Scandinavia, *J. Geophys. Res.*, *107*(D20), 8287, doi:10.1029/2001JD000452.

Drdla, K., and M. R. Schoeberl (2003), Microphysical modeling of the 1999–2000 Arctic winter: 2. Chlorine activation and ozone depletion, *J. Geophys. Res.*, *108*(D5), 8319, doi:10.1029/2001JD001159.

Dudhia, J. (1993), A non-hydrostatic version of the Penn State-NCAR Mesoscale Model: Validation tests and simulation of an Atlantic cyclone and cold front, *Mon. Weather Rev.*, *121*, 1493–1513.

Dudhia, J., D. Gill, Y.-R. Guo, K. Manning, and W. Wang (2001), PSU/NCAR Mesoscale Modeling System tutorial class notes and user guide: MM5 Modeling System Version 3, Natl. Cent. for Atmos. Res., Boulder, Colo. (Available at http://www.mmm.ucar.edu/mm5/doc.html)

Enell, C., A. Steen, T. Wagner, U. Frieß, K. Pfeilsticker, U. Platt, and K.-H. Fricke (1999), Occurrence of polar stratospheric clouds at Kiruna, *Ann. Geophys.*, *17*, 1457–1462.

Engel, A., M. Strunk, M. Müller, H.-P. Haase, C. Poss, I. Levin, and U. Schmidt (2002), Temporal development of total chlorine in the high-latitude stratosphere based on reference distributions of mean age derived from CO_2 and SF_6, *J. Geophys. Res.*, *107*(D12), 4136, doi:10.1029/2001JD000584.

Fitzenberger, R. (2001), Investigation of the stratospheric inorganic bromine budget for 1996–2000: Balloon-borne measurements and model comparisons, Ph.D. thesis, Univ. of Heidelberg, Heidelberg, Germany.

Fricke, K.-H., K. P. Müller, G. Baumgarten, and J. Siebert (1997), paper presented at 7th Statusseminar des Ozonforschungsprogramm, Bonn, Germany, July.

Hansen, G., T. Svenoe, M. P. Chipperfield, A. Dahlback, and U.-P. Hoppe (1997), Evidence for substantial ozone depletion in winter 1995/96 over northern Norway, *Geophys. Res. Lett.*, *24*, 799–802.

Hanson, D., and K. Mauersberger (1988), Laboratory studies of the nitric acid trihydrate: Implications for the south polar stratosphere, *Geophys. Res. Lett.*, *15*, 855–858.

Harder, H., et al. (1998), Stratospheric BrO profiles measured at different latitudes and seasons: Atmospheric observations, *Geophys. Res. Lett.*, *25*, 3843–3846.

Hitchman, M. H., M. L. Buker, G. J. Tripoli, E. V. Browell, W. B. Grant, T. J. McGee, and J. F. Burris (2003), Nonorographic generation of Arctic polar stratospheric clouds during December 1999, *J. Geophys. Res.*, *108*(D5), 8325, doi:10.1029/2001JD001034.

Kühl, S., T. Wagner, W. Wilms-Grabe, and U. Platt (2002), Stratospheric chlorine activation derived from GOME OClO measurements: Case studies and comparison to SLIMCAT model results, in *Proceedings of the Sixth European Symposium on Stratospheric Ozone, Göteborg, Sweden*, *Air Pollut. Res. Rep. 79*, Eur. Comm., Brussels. (Available at http://www.ozone-sec.ch.cam.ac.uk/EORCU/goteborg.html)

Kühl, S., et al. (2004), Stratospheric chlorine activation in the Arctic winters 1995/96 to 2001/02 derived from GOME OClO measurements, *Adv. Space Res.*, *34*, 798–803.

Labitzke, K. (1999), *Die Stratosphäre*, Springer-Verlag, New York.

Lary, D. J., and J. A. Pyle (1991), Diffusive radiation, twilight and photochemistry, *J. Atmos. Chem.*, *13*, 373–392.

Lefèvre, F., F. Figarol, K. S. Carslaw, and T. Peter (1998), The 1997 Arctic ozone depletion quantified from three-dimensional model simulations, *Geophys. Res. Lett.*, *25*, 2425–2428.

Leutbecher, M., and H. Volkert (1996), Stratospheric temperature anomalies and mountain waves: A three-dimensional simulation using a multi-scale weather prediction model, *Geophys. Res. Lett.*, *23*, 3329–3332.

Leutbecher, M., and H. Volkert (2000), The propagation of mountain waves into the stratosphere: Quantitative evaluation of three-dimensional simulations, *J. Atmos. Sci.*, *57*, 3090–3108.

Lutman, E. R., et al. (1997), Three-dimensional studies of the 1991/1992 northern hemisphere winter using domain-filling trajectories with chemistry, *J. Geophys. Res.*, *102*, 1479–1488.

Manney, G. L., L. Froidevaux, M. L. Santee, R. W. Zurek, and J. W. Waters (1997), MLS observations of Arctic ozone loss in 1996–97, *Geophys. Res. Lett.*, *24*, 2697–2700.

Marquard, L. C., T. Wagner, and U. Platt (2000), Improved air mass factor concepts for scattered radiation differential optical absorption spectroscopy of atmospheric species, *J. Geophys. Res.*, *105*, 1315–1327.

McElroy, M. B., R. J. Salawitch, S. C. Wofsy, and J. A. Logan (1986), Reductions of Antarctic ozone due to synergistic interactions of chlorine and bromine, *Nature*, *321*, 759–762.

McKinney, K. A., J. M. Pierson, and D. W. Toohey (1997), A wintertime in situ profile of BrO between 17 and 27 km in the Arctic vortex, *Geophys. Res. Lett.*, *24*, 853–856.

Molina, L. T., and M. J. Molina (1987), Production of Cl_2O_2 from the self reaction of the ClO radical, *J. Chem. Phys.*, *91*, 433–436.

Müller, R., J.-U. Grooß, D. S. McKenna, P. J. Crutzen, C. Brühl, J. M. Russel III, and A. F. Tuck (1997), HALOE observations of the vertical structure of chemical ozone depletion in the Arctic vortex during winter and early spring 1996–1997, *Geophys. Res. Lett.*, *24*, 2717–2720.

Newman, P. A., J. F. Gleason, R. D. McPeters, and R. S. Stolarski (1997), Anomalously low ozone over the Arctic, *Geophys. Res. Lett.*, *24*, 2689–2692.

Pawson, S., and B. Naujokat (1999), The cold winters of the middle 1990s in the northern lower stratosphere, *J. Geophys. Res.*, *104*, 12,209–12,222.

Pawson, S., et al. (1995), On the polar stratospheric cloud formation potential of the northern stratosphere, *J. Geophys. Res.*, *100*, 23,215–23,225.

Peter, T. (1997), Microphysics and heterogeneous chemistry of polar stratospheric clouds, *Annu. Rev. Phys. Chem.*, *48*, 785–822.

Pierson, J. M., et al. (1999), An investigation of ClO photochemistry in the chemically perturbed Arctic vortex, *J. Atmos. Chem.*, *32*, 61–81.

Platt, U. (1994), Differential Optical Absorption Spectroscopy (DOAS), in *Air Monitoring by Spectroscopic Techniques*, *Chem. Anal. Ser.*, vol. 127, edited by M. W. Sigrist, John Wiley, Hoboken, N. J.

Pommerau, J.-P., and J. Piquard (1994), Observations of the vertical distribution of stratospheric OClO, *Geophys. Res. Lett.*, *21*, 1231–1234.

Rex, M., et al. (2003), On the unexplained stratospheric ozone losses during cold Arctic Januaries, *Geophys. Res. Lett.*, *30*(1), 1008, doi:10.1029/2002GL016008.

Richter, A., et al. (1999), Validation of GOME O_3, NO_2, BrO, and OClO measurements in southern high latitudes, in *Proceedings of Fifth European Workshop on Stratospheric Ozone, St. Jean de Luz, France*, Eur. Comm., Brussels. (Available at http://www.ozone-sec.ch.cam.ac.uk/EORCU/Workshops/Fifthproc.html)

Richter, A., F. Wittrock, M. Weber, S. Beirle, S. Kühl, U. Platt, T. Wagner, W. Wilms-Grabe, and J. P. Burrows (2004), GOME observations of stratospheric trace gas distributions during the splitting vortex event in the Antarctic winter 2002, part I: Measurements, *J. Atmos. Sci.*, in press.

Rivière, E. D., et al. (2000), Role of lee waves in the formation of polar stratospheric clouds: Case studies from February 1997, *J. Geophys. Res.*, *105*, 6845–6853.

Sander, S. P., and R. R. Friedl (1989), Kinetics and product studies of the reaction ClO + BrO using flash photolysis-ultraviolet absorption, *J. Phys. Chem.*, *93*, 4764–4771.

Sander, S. P., et al. (2003), Chemical kinetics and photochemical data for use in stratospheric modeling, evaluation 14, *JPL Publ.*, *02-25*.

Santee, M. L., W. G. Read, J. W. Waters, L. Froidevaux, G. L. Manney, D. A. Flower, R. F. Jarnot, R. S. Harwood, and G. E. Peckham (1995), Interhemispheric differences in polar stratospheric HNO_3, H_2O, ClO, and O_3, *Science*, *267*, 849–852.

Santee, M. L., G. L. Manney, L. Froidevaux, R. W. Zurek, and J. W. Waters (1997), MLS observations of ClO and HNO_3 in the 1996–97 Arctic polar vortex, *Geophys. Res. Lett.*, *24*, 2713–2716.

Santee, M. L., G. L. Manney, J. W. Waters, and N. J. Livesey (2003), Variations and climatology of ClO in the polar lower stratosphere from UARS Microwave Limb Sounder measurements, *J. Geophys. Res.*, *108*(D15), 4454, doi:10.1029/2002JD003335.

Schiller, C., and A. Wahner (1996), Comment on "Stratospheric OClO measurements as a poor quantitative indicator of chlorine activation" by J. Sessler, M. P. Chipperfield, J. A. Pyle, and R. Toumi, *Geophys. Res. Lett.*, *23*, 1053–1054.

Schmidt, U., R. Bauer, A. Engel, R. Borchers, and J. Lee (1994), The variation of available chlorine, Cl_y, in the Arctic polar vortex during EASOE, *Geophys. Res. Lett.*, *21*, 1215–1218.

Sessler, J., M. P. Chipperfield, J. A. Pyle, and R. Toumi (1995), Stratospheric OClO measurements as a poor quantitative indicator of chlorine activation, *Geophys. Res. Lett.*, *22*, 687–690.

Sessler, J., M. P. Chipperfield, J. A. Pyle, and R. Toumi (1996), Reply to C. Schiller and A. Wahner, *Geophys. Res. Lett.*, *23*, 1055.

Sinnhuber, B.-M., et al. (2002), Comparison of measurements and model calculations of stratospheric bromine monoxide, *J. Geophys. Res.*, *107*(D19), 4398, doi:10.1029/2001JD000940.

Solomon, P., B. Connor, J. Barrett, T. Mooney, A. Lee, and A. Parrish (2002), Measurements of stratospheric ClO over Antarctica in 1996–2000 and implications for ClO dimer chemistry, *Geophys. Res. Lett.*, *29*(15), 1708, doi:10.1029/2002GL015232.

Solomon, S. (1999), Stratospheric ozone depletion: A review of concepts and history, *Rev. Geophys.*, *37*(3), 275–316.

Solomon, S., G. H. Mount, R. W. Sanders, and A. L. Schmeltekopf (1987a), Visible spectroscopy at McMurdo Station, Antarctica: 2. Observations of OClO, *J. Geophys. Res.*, *92*, 8329–8338.

Solomon, S., A. L. Schmeltekopf, and R. W. Sanders (1987b), On the interpretation of zenith sky absorption measurements, *J. Geophys. Res.*, *92*, 8311–8319.

Solomon, S., R. W. Sanders, and H. L. Miller (1990), Visible and near-ultraviolet spectroscopy at McMurdo Station, Antarctica: 7. OClO photochemistry and ozone destruction, *J. Geophys. Res.*, *95*, 13,807–13,817.

Stein, B., et al. (1999), Optical classification, existence temperatures, and coexistence of different polar stratospheric cloud types, *J. Geophys. Res.*, *104*, 23,983–23,993.

Stimpfle, R. M., D. M. Wilmouth, R. J. Salawitch, and J. G. Anderson (2004), First measurements of ClOOCl in the stratosphere: The coupling of ClOOCl and ClO in the Arctic polar vortex, *J. Geophys. Res.*, *109*, D03301, doi:10.1029/2003JD003811.

Stutz, J., and U. Platt (1996), Numerical analysis and error estimation of Differential Optical Absorption Spectroscopy measurements least squares methods, *Appl. Opt.*, *35*, 6041–6053.

Terao, Y., Y. Sasano, H. Nakajima, H. L. Tanaka, and T. Yasunari (2002), Stratospheric ozone loss in the 1996/1997 Arctic winter: Evaluation based on multiple trajectory analysis for double-sounded air parcels by ILAS, *J. Geophys. Res.*, *107*(D24), 8210, doi:10.1029/2001JD000615.

Tilmes, S., R. Müller, J.-U. Grooß, D. S. McKenna, J. M. Russel III, and Y. Sasano (2003), Calculation of chemical ozone loss in the Arctic winter 1996–1997 using ozone-tracer correlations: Comparison of Improved Limb Atmospheric Spectrometer (ILAS) and Halogen Occultation Experiment (HALOE) results, *J. Geophys. Res.*, *108*(D2), 4045, doi:10.1029/2002JD002213.

Tornkvist, K. K., D. W. Arlander, and B.-M. Sinnhuber (2002), Ground-based UV measurements of BrO and OClO over Ny-Alesund during winter 1996 and 1997 and Andoya during winter 1998/99, *J. Atmos. Chem.*, *43*, 75–106.

Toumi, R. (1994), Reaction of ClO with NO_3: OClO formation and night-time O_3 loss, *Geophys. Res. Lett.*, *21*(13), 1487–1490.

Vogel, B., et al. (2003), Vertical profiles of activated ClO and ozone loss in the Arctic vortex in January and March 2000: In situ observations and model simulations, *J. Geophys. Res.*, *108*(D22), 8334, doi:10.1029/2002JD002564.

Voigt, C., et al. (2000), Nonequilibrium compositions of liquid polar stratospheric clouds in gravity waves, *Geophys. Res. Lett.*, *27*(23), 3873–3876.

Voigt, C., et al. (2003), In situ mountain-wave polar stratospheric cloud measurements: Implications for nitric acid trihydrate formation, *J. Geophys. Res.*, *108*(D5), 8331, doi:10.1029/2001JD001185.

Wagner, T., C. Leue, K. Pfeilsticker, and U. Platt (2001), Monitoring of the stratospheric chlorine activation by Global Ozone Monitoring Experiment (GOME) OClO measurements in the austral and boreal winters 1995 through 1999, *J. Geophys. Res.*, *106*, 4971–4986.

Wagner, T., F. Wittrock, A. Richter, M. Wenig, J. P. Burrows, and U. Platt (2002a), Continuous monitoring of the high and persistent chlorine activation during the Arctic winter 1999/2000 by the GOME instrument on ERS-2, *J. Geophys. Res.*, *107*(D20), 8267, doi:10.1029/2001JD000466.

Wagner, T., S. Beirle, C. v. Friedeburg, J. Hollwedel, S. Kraus, M. Wenig, W. Wilms-Grabe, S. Kühl, and U. Platt (2002b), Monitoring of trace gas emissions from space: Tropospheric abundances of BrO, NO_2, H_2CO, SO_2, H_2O, O_2, and O_4 as measured by GOME, in *Air Pollution 2002*, vol. 10, pp., 463–472, WIT Press, Billerica, Mass.

Wahner, A., G. Tyndall, and A. Ravishankara (1987), Absorption cross sections for OClO as a function of temperature in the wavelength range from 240–490 nm, *J. Phys. Chem.*, *91*, 2735–2738.

Weber, M., S. Dhomse, F. Wittrock, A. Richter, B.-M. Sinnhuber, and J. P. Burrows (2003), Dynamical control of NH and SH winter/spring total ozone from GOME observations in 1995–2002, *Geophys. Res. Lett.*, *30*(11), 1583, doi:10.1029/2002GL016799.

Wernli, H., and H. C. Davis (1997), A Lagrangian-based analysis of extratropical cyclones. I: The method and some applications, *Q. J. R. Meteorol. Soc.*, *123*, 467–489.

Wilms-Grabe, W., et al. (2002), Monitoring of stratospheric chlorine activation with GOME OClO measurements, in *Proceedings of Sixth European Symposium on Stratospheric Ozone, Gothenburg, Sweden*, *Air Pollut. Res. Rep. 79*, Eur. Comm., Brussels. (Available at http://www.ozone-sec.ch.cam.ac.uk/EORCU/goteborg.html)

Wirth, M., et al. (1999), Model-guided Lagrangian observation and simulation of mountain polar stratospheric clouds, *J. Geophys. Res.*, *104*, 23,971–23,981.

Wittrock, F., A. Richter, and J. P. Burrows (1999), Validation of GOME BrO and OClO observations in the northern hemisphere, paper presented at European Symposium on Atmospheric Measurements From Space (ESAMS 99), Eur. Space Agency, Noordwijk, Netherlands.

Woyke, T., R. Müller, F. Stroh, D. S. McKenna, A. Engel, J. J. Margitan, M. Rex, and K. S. Carslaw (1999), A test of our understanding of the ozone chemistry in the Arctic polar vortex based on in situ measurements of ClO, BrO, and O_3 in the 1994/1995 winter, *J. Geophys. Res.*, *104*(D15), 18,755–18,768.

Zängl, G. (2002), Stratified flow over a mountain with a gap: Linear theory and numerical simulations, *Q. J. R. Meteorol. Soc.*, *128*, 927–949.

A. Dörnbrack, Institut für Physik der Atmosphäre, DLR Oberpfaffenhofen, D-82230 Wessling, Germany. (andreas.doernbrack@dlr.de)

S. Kühl, U. Platt, T. Wagner, and W. Wilms-Grabe, Institut für Umweltphysik, Universität Heidelberg, Im Neuenheimer Feld 229, D-69120 Heidelberg, Germany. (skuehl@iup.uni-heidelberg.de)

B.-M. Sinnhuber, Institut für Umweltphysik, Universität Bremen, D-28334 Bremen, Germany. (bms@iup.physik.uni-bremen.de)